AMERICAN SOCIETY FOR METALS
Metals Park, Ohio 44073

Metals/Materials Technology Series

THE FORMATION OF ANNEALING TWINS: OVERVIEW AND NEW THOUGHTS

Marc A. Meyers
New Mexico Institute of Mining & Technology
Socorro, New Mexico 87801, USA
and
U.S. Army Research Office
Research Triangle Park, NC 27709, USA

Christian McCowan
Colorado School of Mines
Golden, Colorado 80401, USA

International Symposium on
Interface Migration and Control or Microstructure
held in conjunction with
ASM's Metals Congress and TMS/AIME Fall Meeting
Detroit, Michigan, USA
17-21 September 1984

8408-037

8408-037

THE FORMATION OF ANNEALING TWINS: OVERVIEW AND NEW THOUGHTS

Marc A. Meyers
New Mexico Institute of Mining & Technology
Socorro, New Mexico 87801, USA
and
U.S. Army Research Office
Research Triangle Park, NC 27709, USA

Christian McCowan
Colorado School of Mines
Golden, Colorado 80401, USA

THE FORMATION OF ANNEALING twins has been the object of studies for over fifty years. Mechanisms of formation include growth accident, grain encounter, stacking faults/packets nucleating at grain boundaries, and grain-boundary dissociation. These various mechanisms are reviewed and compared with experimental observations. More recent analyses and measurements suggest that the formation of annealing twins is not completely understood yet.

1. INTRODUCTION

In 1926, Carpenter and Tamura [1] proposed the first mechanism for the formation of annealing twins. Today, sixty years after their papers, most metallurgists do not have a clear understanding of their formation, in spite of the voluminous literature devoted to the subject. Why? As a graduate student (a dozen years ago), one of the authors (MAM) observed, in a nickel-base superalloy, the profuse parallel bands in an optical microscope. I turned to my fellow student, Dick Salzbrenner, and asked him: "How are they formed?". He answered in his typical self-assured manner: "It is obvious that every textbook has the explanation, Meyers!". So we went to the textbook, which showed the classic growth accident picture (Fig. 9 in this paper). But the picture obviously did not explain why, most of the time, parallel lines were observed (twin twins?). Figure 1 shows the annealing twins in copper. Clearly, only four single-sided twins are observed, while thirteen parallel-sided twins are seen. So, we proceeded in our search through other textbooks. Invariably, we found the same picture, and everybody agreed that the growth accident model was a true representation of the formation of annealing twins. This led to a more thorough search and the realization that none of the existing models was entirely satisfactory. In these past dozen years, the understanding of annealing twins has improved considerably, as will become evident from this overview. Annealing twins are truly fascinating, and ever present in FCC metals. The reason why they did not receive the focussed attention that martensitic transformation, precipitation, and dislocations have is that they do not affect the more mundane properties of metals, such as mechanical strength, significantly. Thus, the neglect, induced by economical reasoning. The key to an enhanced understanding of annealing (recrystallization, grain-growth, and solidification) twins lies in: (a) in-situ high voltage transmission electron microscopy; (b) quantitative measurement of annealing twin densities as a function of material parameters (grain size, stacking fault energy, etc); and (c) the development of predictive models. In this overview the morphology and structure of twins will be described first; the observations in the various systems will then be reviewed. Next, the four different schools-of-thought explaining their formation are described. Exciting new observations leading to a better understanding are described, quantitative measurements of annealing twin densities are presented, and a modified growth accident model is introduced. Finally, a few comments are made on the icosahedral phase.

2. MORPHOLOGY, STRUCTURE, AND SYSTEMS

Annealing twins are usually observed in optical and transmission electron microscopy, although ion emission microscopy has been used to study them [2,3]. The intersections of an annealing twin with the surface of the specimen form the shapes presented in Figure 2(a). The commonly observed morphologies are one-sided twin (A), complete parallel-sided twin (B), incomplete parallel-sided twin (C), and central twin (D). The same annealing twin could give rise to the four different morphologies, as illustrated in Figure 2(b). It shows a three-dimensional representation of an incomplete parallel-sided twin. Different sectioning planes generate different morphologies. The only correct way to establish twin morphology is

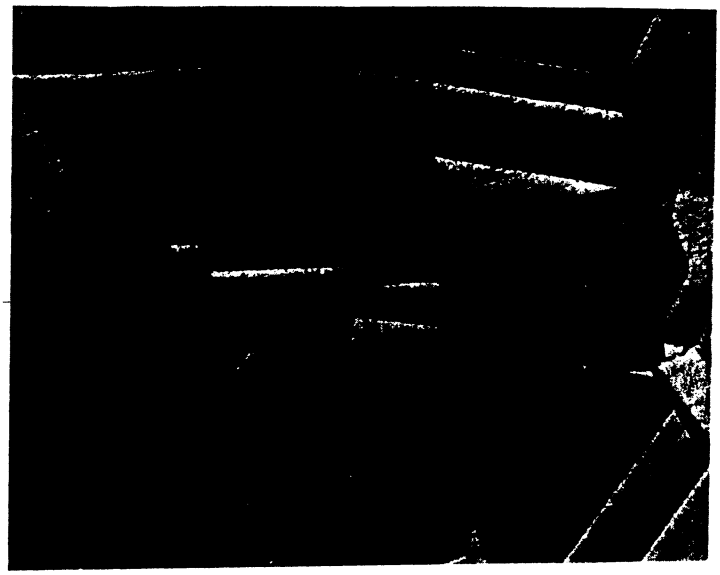

Fig. 1 - Microstructure of copper, showing profuse twinning.

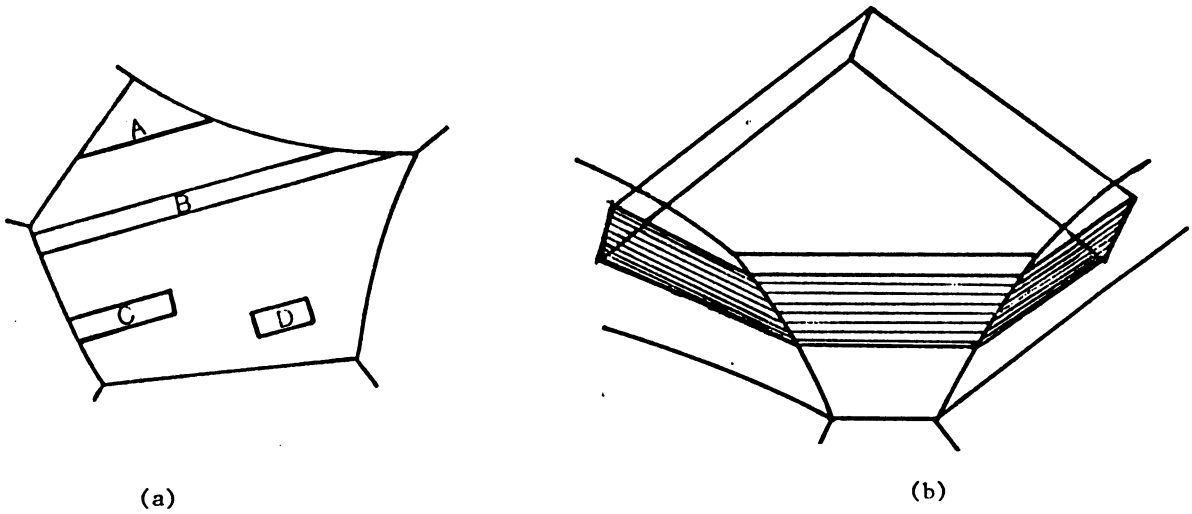

(a) (b)

Fig. 2 - (a) Morphologies of anealing twins observed; A - one-sided twin, B - complete parallel-sided twin, C - incomplete parallel-sided twin, D - central twin; (b) three-dimensional view of parallel-sided twin.

by successive sections of a specimen. To the authors' knowledge, this has not been done, to the present moment. Figure 3 shows the four common morphologies in nickel specimens. These specimens were annealed for 1 hour at 1100°C, then electropolished to remove the surface layers. The four shapes sketched in Figure 2(a) can be clearly seen. In addition to these four morphologies, atypical twins are also observed. While the mechanisms proposed in the next section address mostly the typical twins, no attempt is made here to explain atypical morphologies. Figure 4(a) shows two coherent annealing twin boundaries that meet at a grain boundary, forming a "quadruple" point. Figure 4(b) shows one parallel-sided twin inside a broader one. The two annealing twins are not parallel, but form an angle of approximately 13 degrees, in the plane of the section. Figure 4(c) shows a grain-interior twin (central twin) which offsets a one-sided twin. The evolutionary steps leading to these three morphologies are not understood.

Annealing twins are most commonly observed in FCC metals and alloys. In this lattice, the twin boundary has been identified as a (111) plane. This boundary is called coherent twin boundary and is a symmetric boundary. The angle between the coherent twin boundary and the (111) in the two grains is 70.54°. The coherent twin boundaries terminate, in incomplete parallel sided twins, at an non-coherent boundary. Both

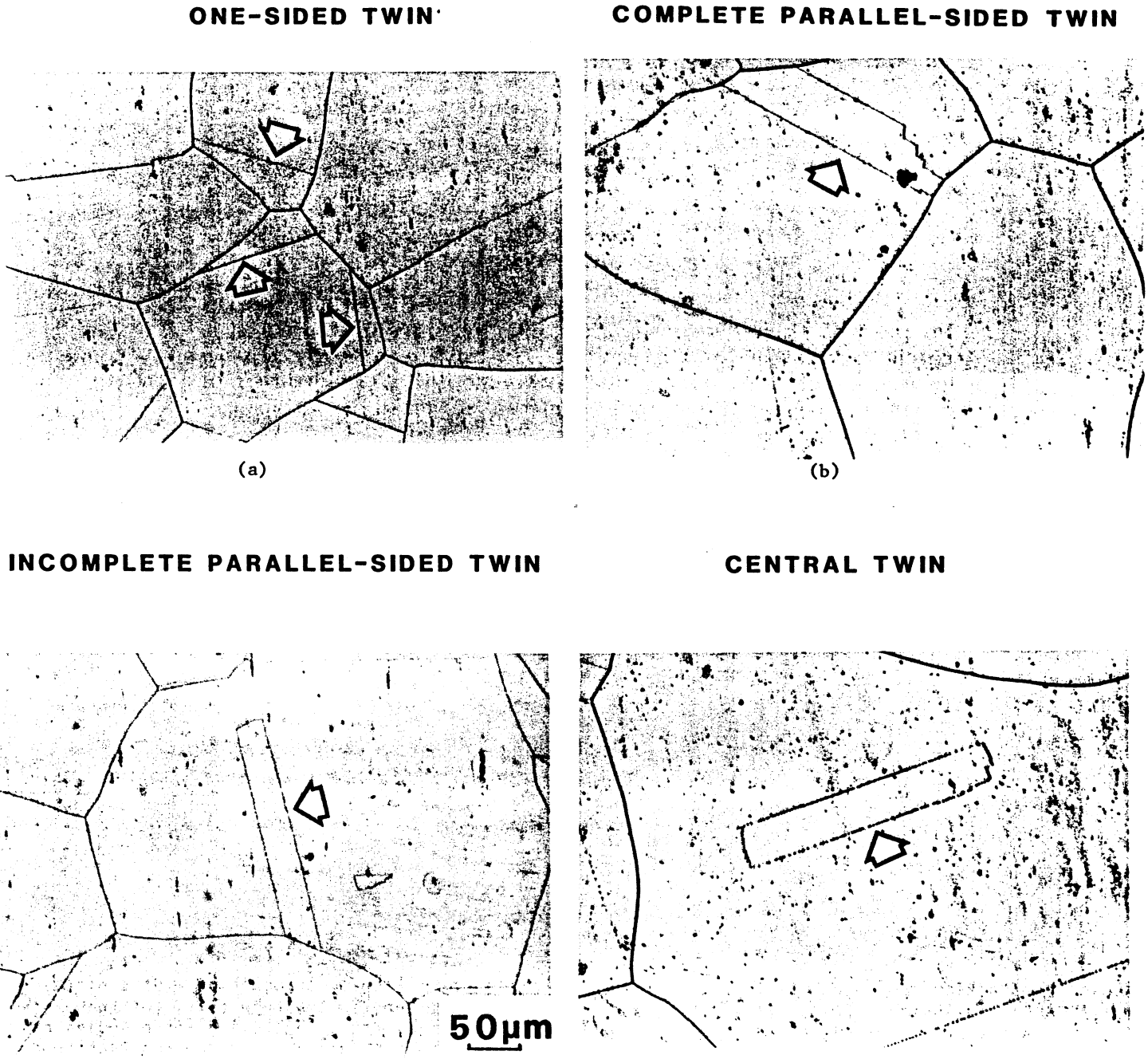

Fig. 3 - Typical annealing twin morphologies observed in nickel.

boundaries are shown in Figure 5(a). These non-coherent boundaries seem to also have preferred orientations; Fullman [4] established that, in copper, the non-coherent twin boundary was approximately parallel to a {113} plane of one crystal and to a {335} of the other. Sargent [5] later identified non-coherent boundaries as {551}, {711} and {211}. Howell and Bee [6] found them to be {113} (matrix) and {335} (twin) or {117} (matrix) and {551} (twin). Dash and Brown [47] identified them as {153}, {110}, and {353}. Vaughn [7] found them to be parallel to {5,5,13} of matrix and {7,7,11} of twin and {110} (both matrix and twin).

The non-coherent boundaries are also "special" boundaries , possessing an energy that is a fraction of random boundaries. They are therefore called more properly semicoherent boundaries. The relationship between the adjacent grains is such that the stacking sequence in the FCC structure is changed. Figure 5(b)

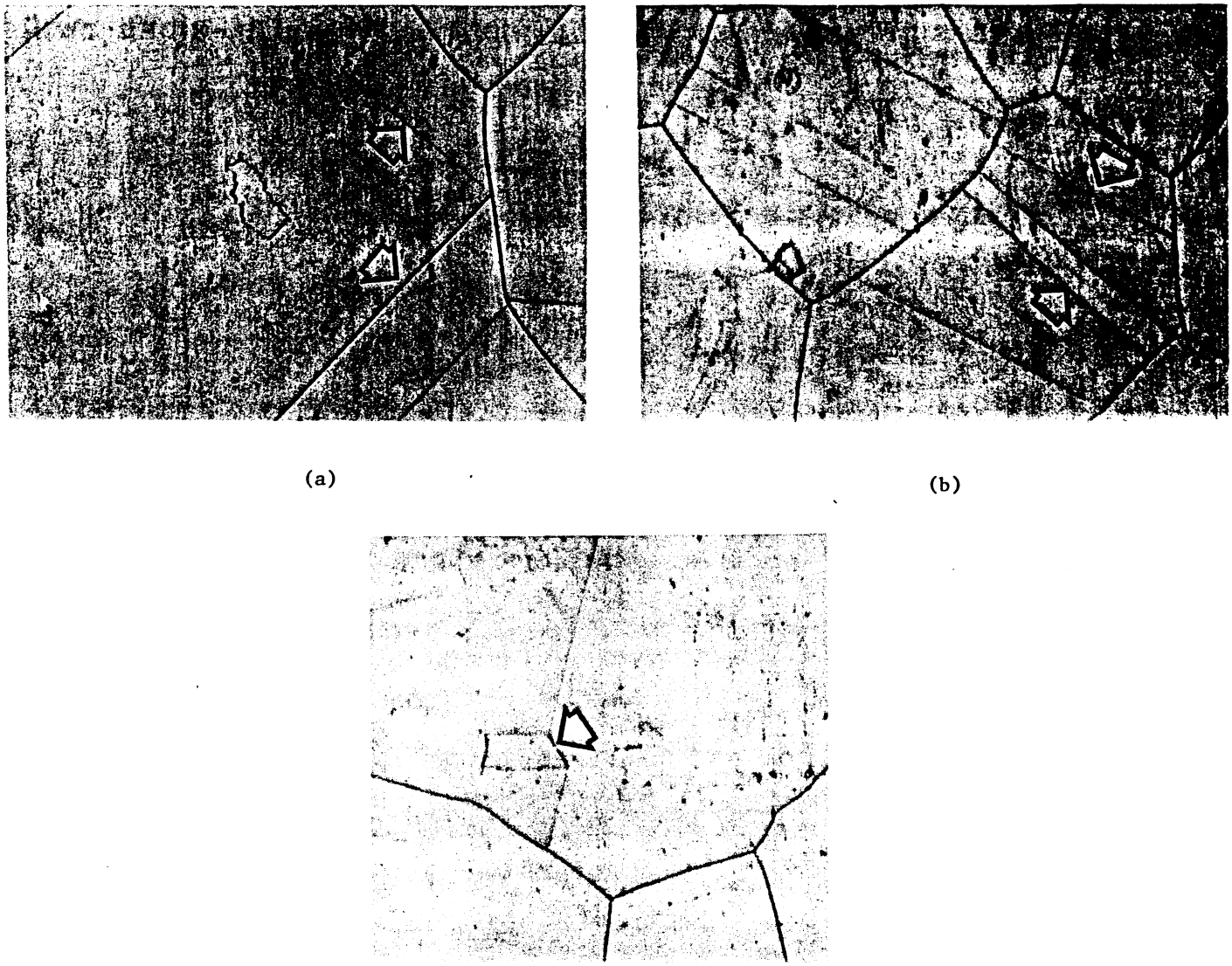

(a) (b)

(c)

Fig. 4. Atypical twins.

shows the stacking sequence outside a twin (normal ABCABC) and inside a twin. It can be seen that it is inverted from ABC to CBA; thus, plane B (the twin plane) is a mirror plane. We therefore have the three-layer region ABA where one can consider the stacking as characteristic of the hexagonal close-packed structure. The interfacial energy of a coherent twin boundary can therefore be expressed as the difference between the free energy of a three-layer HCP structure and the free energy of a FCC structure. This is equal to one half the stacking fault energy of the material. One way of determining the coherent twin-boundary energy is to determine the angles that are made at the intersection of a grain boundary. This problem was successfully tackled by Murr [8,9], who pointed out, correctly, that the dihedral angle between twin and grain boundaries has to be corrected from the direct measurements made on a section. He was able to do this by transmission electron microscopy, by taking the projection widths of the boundary planes in the thin foils (of known/estimated thickness). Table I gives energies of coherent twin boundaries and non-coherent twin boundaries as a function of random grain boundaries. Murr's technique of determining the twin-boundary energies is detailed below. For a single twin boundary - grain boundary intersection, the simple equation relating interfacial free energies and angles can be used (from soap-bubble model). Hence, in Figure 6(a), we have:

$$\gamma_{tb} = - (\gamma_{AB} \cos \Omega_A + \gamma_{T_AB} \cos \Omega_{T_A}) \qquad (1)$$

γ_{tb} is the coherent twin boundary energy; γ_{AB} and γ_{T_AB} are boundary energies. Since both the AB and T_AB boundaries are random (high energy) boundaries, their energies can be taken as e-

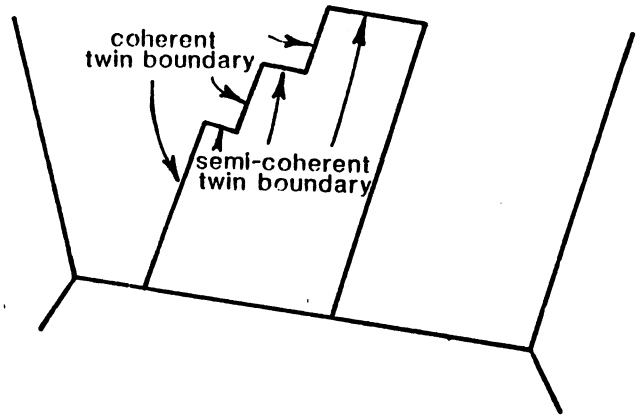

(a)

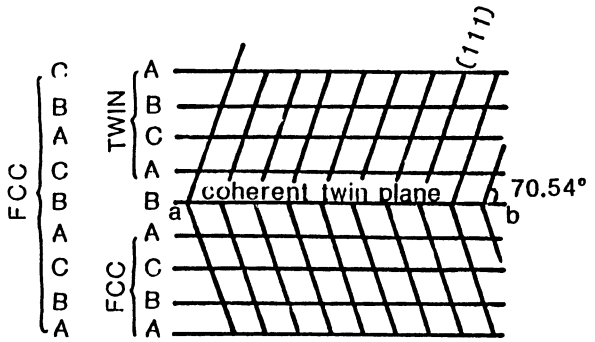

(b)

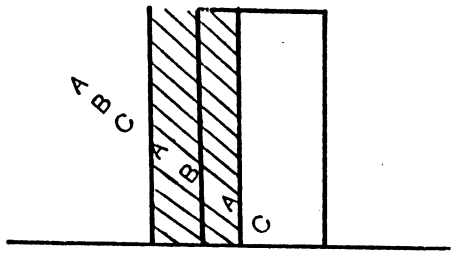

(c)

Fig. 5 - (a) Coherent and non-coherent (or semi-coherent) twin boundaries; (b) Coherent twin boundary; mirror plane B and inversion of stacking sequence in annealing twin; (c) HCP layer formed at annealing twin.

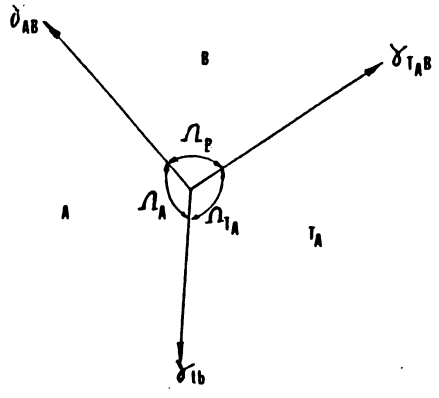

(a)

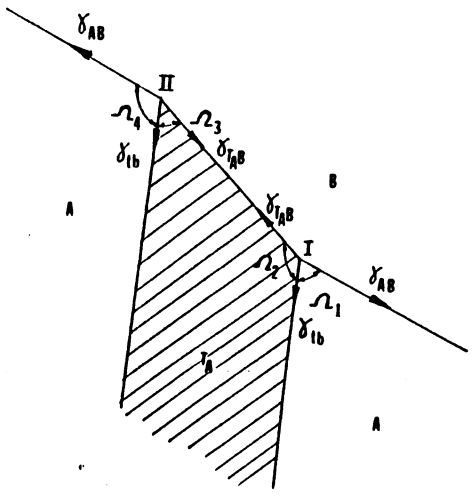

(b)

Fig. 6 - Grain and twin-boundary intersections; (a) interfacial energies for intersection of twin boundary (γ_{tb}) with grain boundary (γ_{AB}, γ_{T_AB}) between grains A and B; (b) interfacial energies for intersection of parallel-sided twin boundary (γ_{tb}) with grain boundary (γ_{AB}, γ_{T_AB}).

qual. The dihedral angles Ω_A and Ω_{T_AB} are also equal.

$$\gamma_{tb} \simeq 2\gamma_{gb} \cos \Omega_B/2 \quad (2)$$

γ_{gb} is the energy of a high angle (random) boundary. For the more complicated situation of the intersection of a parallel-sided annealing twin with a grain boundary, one has the configuration shown in Figure 6(b). This is the experimentally-observed configuration. Murr [8,9] introduced the concept of torques I and II acting at the triple points. The two equilibrium equations are:

$$\gamma_{tb} + \gamma_{AB} \cos \Omega_1 + \gamma_{T_AB} \cos \Omega_2 + \Sigma M_I = 0 \quad (3)$$

$$\gamma_{tb} + \gamma_{AB} \cos \Omega_4 + \gamma_{T_AB} \cos \Omega_3 + \Sigma M_{II} = 0 \quad (4)$$

The torques M_I and M_{II} are due to the orientation dependence of the grain boundary energy:

$$\Sigma M_I = \frac{\partial \gamma_{AB}}{\partial \Omega} \sin\Omega_1 + \frac{\partial \gamma_{TAB}}{\partial \Omega} \sin\Omega_2 \quad (5)$$

$$\Sigma M_{II} = \frac{\partial \gamma_{AB}}{\partial \Omega} \sin\Omega_4 + \frac{\partial \gamma_{TAB}}{\partial \Omega} \sin\Omega_3 \quad (6)$$

The derivation above shows how the energies in Table I were estimated. The annealing twin frequency is strongly dependent on the ratio γ_{tb}/γ_{gb}. As an example, while aluminum has less than 10^{-3} twin boundaries/grain (γ_{tb}/γ_{gb} = 0.23), nickel has ~ 1 twin boundary/grain (γ_{tb}/γ_{gb}=0.05).

TABLE I

Energies of coherent (γ_{tb}) and non-coherent (γ_{ntb}) grain boundaries as a function of grain-boundary energies (γ_{gb}); stacking-fault energies also given. (Adapted from L. E. Murr, Interfacial Phenomena in Metals, Addison Wesley, Reading, Mass., Tables 2.1, 3.6, and 3.9).

Metal	γ_{gb} (erg/cm^2)	γ_{sf} (erg/cm^2)	γ_{tb}/γ_{gb}	γ_{ntb}/γ_{gb}
Al	324	166	0.23	
Cu	625	78	0.035	0.80
Cu-5 a/o Al		20	0.032	0.32
Au	378	45	0.039	
SS(304)	835	21	0.024	0.25
Ni	866	128	0.050	
Ag	375	22	0.030	0.33

The structure of the non-coherent (or semi-coherent) annealing twin boundaries has not been incontrovertibly identified, to these authors' knowledge. Two models for the structure have been proposed, and are shown in Figure 7. Oblak and Kear [10] in 1970 suggested that, because of the simple crystallographic relationship between matrix and twin in FCC materials, this boundary could be thought of in terms of dislocation arrays. They analyzed, by TEM, two possibilities: arrays of 1/6 [112] Shockley partials and of 1/3 [111] Frank partials. These arrays would be responsible for creating a twin configuration. By means of special procedures in the TEM, they ruled out the Shockley partials, concluding that the boundary consisted of the Frank partials shown in Figure 7(a). Meyers and Murr [11], on the other hand, arrived at a different proposed array from the model. The dislocations are Shockley partials, but oriented differently them Oblak and Kear's dislocations (rotated 90° to their dislocations). The general condition is the same: the total Burgers vector of the interface is zero, since no strain is involved in an annealing twin. Figure 7(b) shows the interface proposed by Meyers and Murr [11]. This specific array it required in their model, to make the non-coherent boundary glissile. The dislocation arrangement is such that it changes the matrix to the twin stacking sequence. The dislocations are associated pair-wise with opposite signs, forming dipoles. Since the planes labeled C are not affected by twinning, there is no need for dislocations in them. The strain energy of the individual dislocations within the dipoles is minimized if they position themselves at an angle in the vicinity of 45°, as shown in Figure 7(b). The relative position of the individual dipoles will also be such as to minimize the energy. This energy minimum should coincide with the "special" boundary inclinations reported earlier.

Annealing twins have been reported in many metals and alloys. The FCC, BCC, and diamond cubic structures are represented. Ti O_2 is a ceramic in which twins have been unmistakenly identified by Carr [12]. Figure 8 shows a transmission electron micrograph and the electron diffraction pattern. Two parallel-sided twins are clearly seen in adjacent grains. The diffraction pattern shows both the matrix and twin reflections. However, most of the annealing twin observations have been made on FCC materials. Table II provides a listing (certainly, incomplete) of annealing twin observations. While most FCC metals and alloys with reasonably low stacking-fault energy exhibit annealing twins, there are only a few reports of these twins in other structures. Viltange [28] reports the formation of twins during the growth of iron single crystals of high purity. Saleeb and Kadeckova [25] report that the density of these twin boundaries produced in strain annealing iron to produce single crystals decreases drastically with small additions of silicon. Wasilewski [32] reports annealing twins in nio-

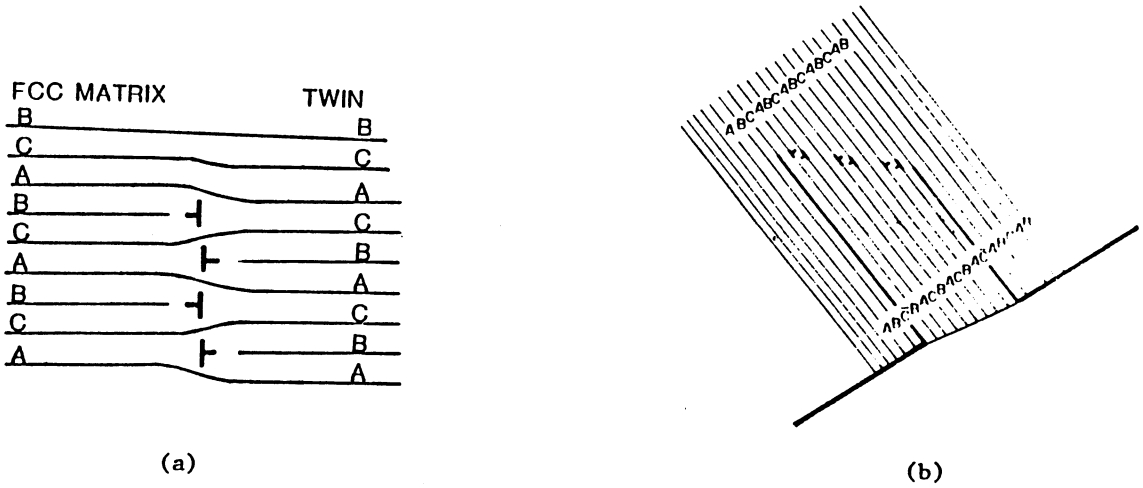

Fig. 7 - Models for non-coherent (or semi-coherent) twin boundaries; (a) Oblak and Kear; (b) Meyers - Murr.

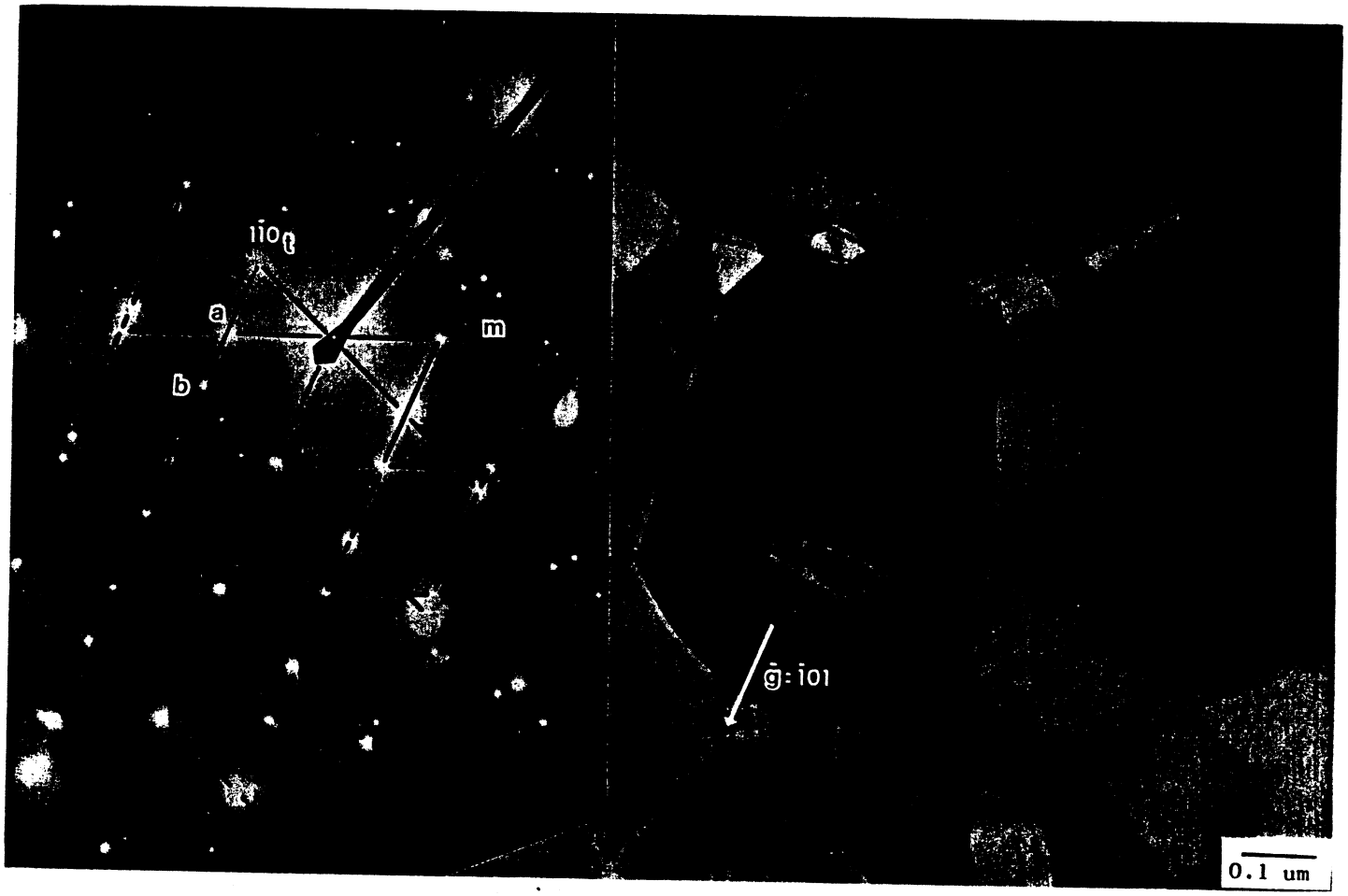

Fig. 8 - Annealing twin (parallel-sided) and its diffraction pattern in TiO_2 (Courtesy of M. J. Carr, Sandia National Laboratories).

TABLE II

Systems in Which Annealing Twins Have Been Identified

System	Investigator	Year
FCC		
Ag	Kosevich et al	1978
Al and alloys	Gleiter	1969
	Murr	1973
	Gastaldi and Jourdan	1979
	Pankin et al	1980
Au	McGinn et al	1982
Austenitic SS		
Brass	Bay et al	1972
Cu; Cu-Zn; Cu-Sn; Cu-Ga; Cu-Al	Numerous reports	
Ni; Ni-Co; Ni-Fe; superalloys	Numerous reports	
Pb;	Parameswaran and Weertman	1969
	Tardy and Iskander	1969
	Eady and Winegard	1974
Pb-Ag; Pb-Tl; Pb-Au	Simpson et al	1970
$L1_2$ ordered intermetallics		
Ni_3Al	Schulsen et al	1985
$(Fe, Co, Ni)_3V$	Liu	1985
Fe_3Al	Cahn and Cohl	1961
Zr_3Al	Schulson	1984
BCC		
Fe	Saleeb and Kadeckova	1974
Fe(high purity)	Hutton et al	1959
	Foudreux and Berghzan	1960
	Simonsen	1962
	Viltange	1975
Nb	Wasilewski	1966
Diamond Cubic		
Si	Borle	1973
	Ohdomari and Onoda	1977
	Guy and Hren (p. 302)	
TiO_2	Carr	1985

bium, but a close examination of his paper shows that there is no real proof; there is indication that adjacent grains have a twin orientation. BCC materials are known to form mechanical twins readily; so are HCP materials. Low-temperature and high-strain rate deformation, for which thermal activation is severely reduced, tends to lead to deformation twinning.

Intermetallic compounds with the $L1_2$ structure exhibit parallel-sided annealing twins. Observations are reported by Schulson et al. [24] for Ni_3Al, Schulson [27] for Zr_3Al, and Liu [20] for $(Fe, Co, Ni)_3V$. These intermetallics have an FCC structure with a BCC superlattice. Annealing twins have also bee observed in silicon and germanium; observations in germanium and dissociation of a grain boundary are reported by Z. Elgat ("Structure of Twin Boundaries in Ge and Spinel", Ph. D. Thesis, Cornell U., 1985, MSC Report 5644).

So, one can conclude that annealing twin formation is a phenomenon typical of FCC metals and alloys. It is not typical of BCC and HCP structures and some ceramic structures might exhibit them. Annealing twins are observed in numerous minerals, but will not be discussed here.

3. MECHANISMS FOR FORMATION OF ANNEALING TWINS

By reviewing the literature one may find over ten proposed models for the formation of annealing twins. Upon closer examination, these various models can be grouped into four schools-of-thought. Of these, only the model by Gleiter allows a theoretical prediction of twin densi-

ties. Hence, the name theory is only used for Gleiter, since it infers a predictive capability verified by experiments. Table III presents, in a very summarized way, the main contributions to the theoretical framework on annealing twins. These models can be grouped into (a) growth accident; (b) grain encounter; (c) stacking-fault packets at migrating grain boundaries; and (d) grain-boundary dissociation. These models are described below.

TABLE III

Mechanisms For Formation

- Growth Accident
  Carpenter and Tamura (1926), Burke (1950), Fullman and Fisher (1951), Gleiter (1969)
- Grain Encounter
  Burgers (1946, 1949), Nielsen (1967)
- Stacking-Fault Packets At Migrating Grain Boundaries
  Dash and Brown (1963)
- Grain Boundary Dissociation
  Meyers and Murr (1978)
  Goodhew (1979)

3.1 GROWTH ACCIDENT MODEL - This model was proposed in 1926 by Carpenter and Tamura [1] and in a more detailed way by Burke [37] and Fullman and Fischer [40]. Gleiter [38] presented an atomistic interpretation and developed predictive equations. Figure 9 shows the sequence of formation of two annealing twin boundaries by this mechanism. The two grain boundaries are migrating to the right in Figure 9(a). If there is a decrease in the overall energy, the fault that occurs in (b) is stable. The twinned area grows with increased grain-boundary migration. The formation of the annealing twin creates the following energetic unbalance:

$$\gamma_{tb} A_{12} + \gamma'_{13} A_{13} + \gamma'_{23} A_{23} < \gamma_{13} A_{13} + \gamma_{23} A_{23} \qquad (7)$$

The primes(') indicate the energies after the formation of the twin. If a second growth accident occurs (Figure 9(d)), then one has a parallel-sided twin. According to this model, the two sides of a parallel-sided twin are produced by two completely independent events. Thus, the average distance between two annealing twin boundaries is equal to the average distance between two twins. This is obviously not the case. Nevertheless, aluminum has only been known to exhibit grain-corner twins, and this model satisfactorily addresses this material. Gleiter [38,39] presented an atomistic model for the growth accident. He based it on the idea that grain boundaries migrate by a ledge mechanism. A lateral migration of a ledge produces a forward movement of the boundary. Figure 10 shows, schematically, the process of grain-boundary migration; grain I is shrinking at the expense of grain II. The boundary is seen as a sequence of steps on close-packed planes: ab, bf, fg, gh. Atoms migrate from the step edges (ledges) of grain I to the ends of the ledges in grain II, as indicated by arrows. These close-packed planes are assumed to be {111}. At lm a stacking accident occurs so that the stacking sequence is faulted. Hence the level i k is at a stacking fault, creating a coherent twin boundary. Gleiter [38,39] calculated the probability that a {111} plane was a coherent twin boundary.

$$P = \exp \left\{ \frac{-Q/kT + \ln (\Delta G / k T)}{(\pi \varepsilon^2 \quad h^2 / Q \gamma_{tb}) - 1} \right\} \qquad (8)$$

T is the temperature in K, Q is the activation energy for grain-boundary migration, ΔG is the critical free energy for the formation of a twin nucleus at a boundary; ε is the energy of a step; h is the height of the twin nucleus; γ_{tb} is the energy of a coherent twin boundary. From this equation Gleiter [38,39] was able to determine the effect of temperature on twin probability. This probability was converted into a twin density, defined by Gleiter as the density of twins intersecting a straight line on the surface (linear intercept). Figure 11 shows the prediction of Gleiter's theory compared to experimental results. The parameter ε was adjusted to provide the fit. The experimental results are for Cu- 3 wt%Al at a constant grain size of 300μm. This reviewer espouses Pande, Iman and Rath's [41] comments that the twin density could be assumed constant (if one considers the scatter of the data) at approximately 3×10^{-5}. Gleiter's theory predicts an increase in twin density (measured as twins/micrometer) with increasing temperature. McGinn et al. [18,42] found support for Gleiter's theory in the interpretation of annealing twin formation in small particles. Baro and Gleiter [39] concluded that below 600°C another (or an additional) annealing twin formation mechanism was operating.

3.2 GRAIN ENCOUNTER MODEL - This model is generally credited to Nielsen [43], although Burgers proposed a fairly similar concept: the stimulation model [44,45]. This mechanism is shown in Figure 12. The two hatched grains in Figure 12(a) are at a twin orientation. In the general growth process, boundaries are continuously migrating and the two grains become closer (Figure 12(b)). Upon touching, the boundaries form a coherent twin boundary, which minimizes the energy of the system. The energetics dictates that the configuration observed in Figure 12(d) is achieved. One might intuitively argue that the probability of such an event is very small. Nevertheless, Nielsen calculated it and found it to be very realistic. Khayutin [46] applied Nielsen's [43] theory to metals having a

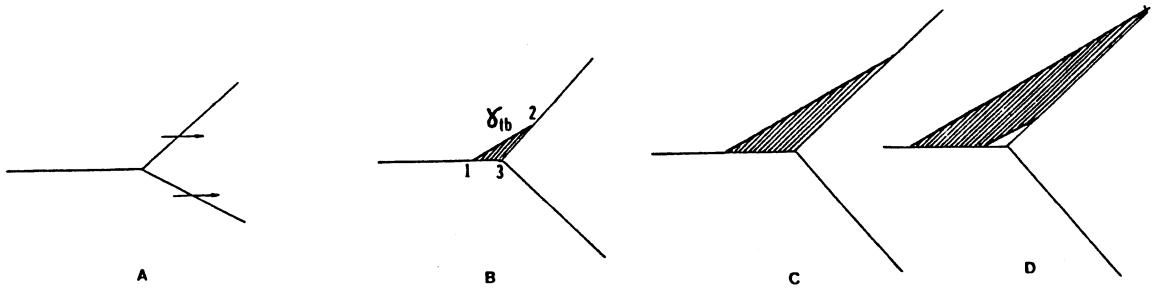

Fig. 9 - Sequence leading to annealing twin formation in growth accident model.

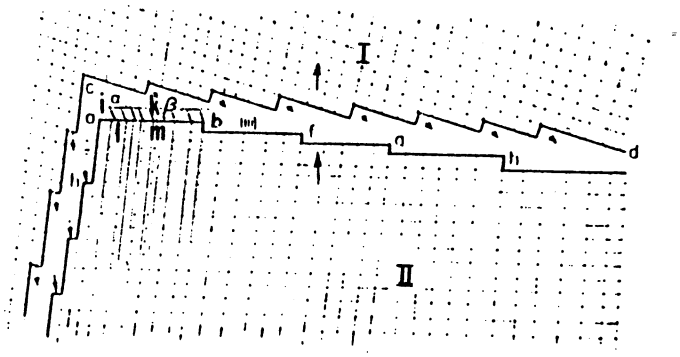

Fig. 10 - Formation of an annealing twin by the nucleation on a close packed plane (a,b). The curved grain boundary moves in the direction of the large arrows, so that crystal II grows (From H. Gleiter, Acta Met., 17, 1421 (1969), Fig. 1).

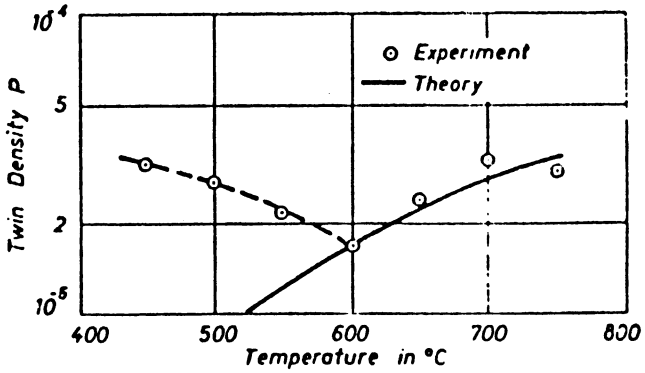

Fig. 11 - The density of annealing twins as a function of temperature (Cu - 3 wt% Al) at constant grain size (300 μm). Theoretical predictions from Greiter's theory come from Eq. 8. (From G. Bäro and H. Gleiter, Z. Metallkde., 63, 661 (1972), Fig. 3).

crystallographic texture, and found that the twins may develop at an average of every third collision between grains with a (311)[112] orientation in low-stacking-fault metals. This number is much higher than Nielsen's original calculation, which showed that the probability that one grain encounter another at a twin orientation was 10^{-4}.

3.3 STACKING FAULT PACKETS AT MIGRATING GRAIN BOUNDARIES - Dash and Brown [47] made transmission electron microscope observations of partially recrystallized specimens and observed annealing twins being formed by mechanisms different than earlier theories. Figure 13 shows the sequence leading to the formation of a parallel-sided twin in a schemetic manner. As the grain boundary moves from right to left, during recrystallization, a packet of stacking faults is formed. This stacking-fault packet coalesces to produce an annealing twin. The growth of the twin proceeds by the movement of the boundary towards the left, by the movement of the non-coherent boundary towards the right, and by the broadening (lateral) of the twin. This broadening is accomplished by the nucleation at the twin-grain-boundary interface. Figure 14 shows transmission electron micrographs substantiating the model presented above. The grain boundary in Figure 14(a) separates the deformed (dark) from the recrystallized material (B) in a Ni-22% Fe alloy. Three annealing twins can be seen. The thickening of the annealing twin occurs by migration of the triple point C. Figure 14(b) shows stacking-fault packets that nucleated at a grain boundary. N_2 indicates the non-coherent steps of these microtwins/stacking fault packets.

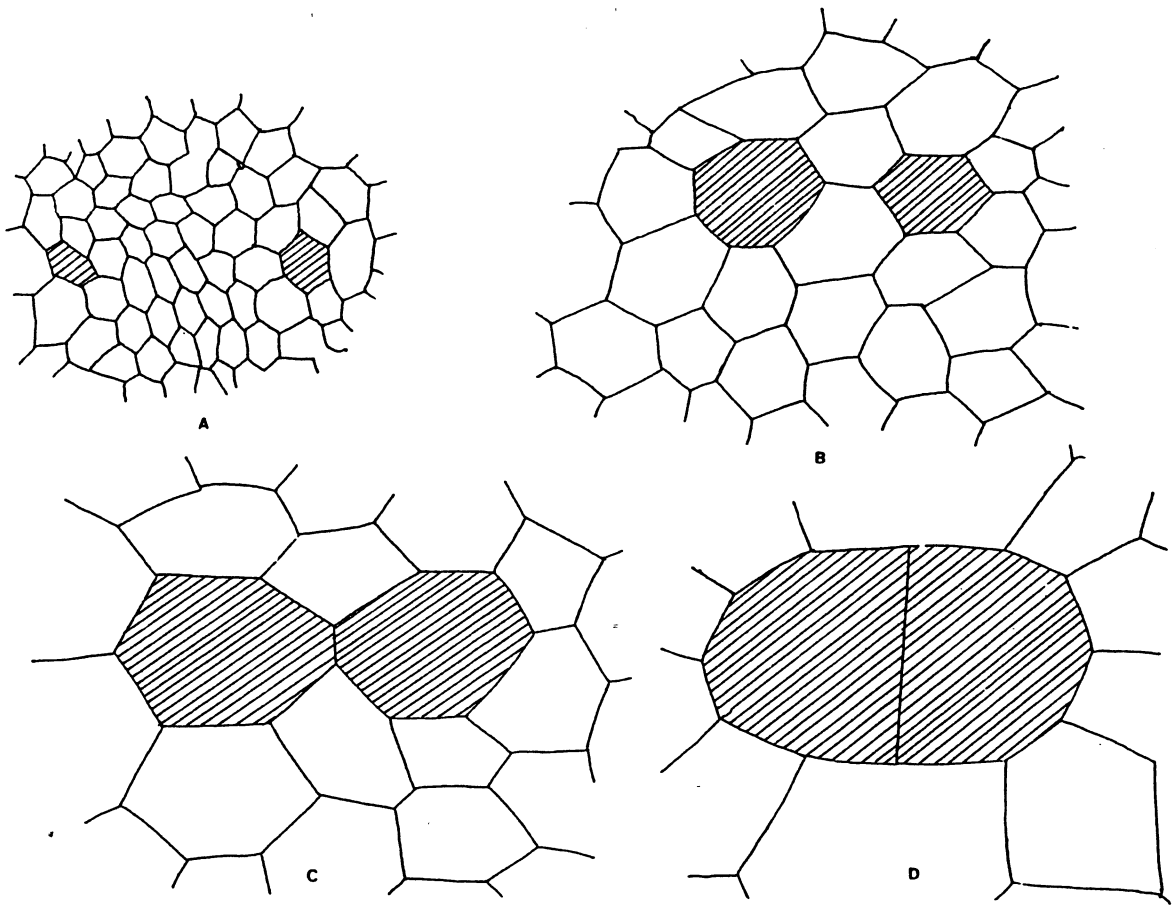

Fig. 12 - Sequence of annealing twin formation by grain encounter mechanism.

STACKING FAULT PACKETS AT MIGRATING GRAIN BOUNDARIES

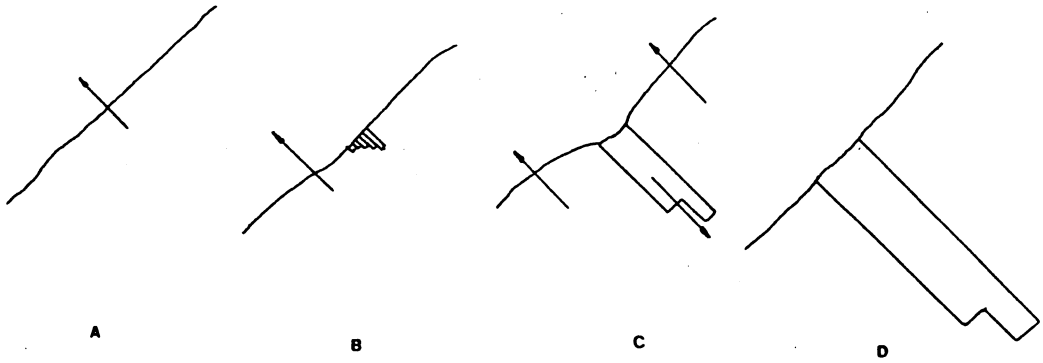

Fig. 13 - Sequence of annealing twin formation by Dash and Brown's mechanism.

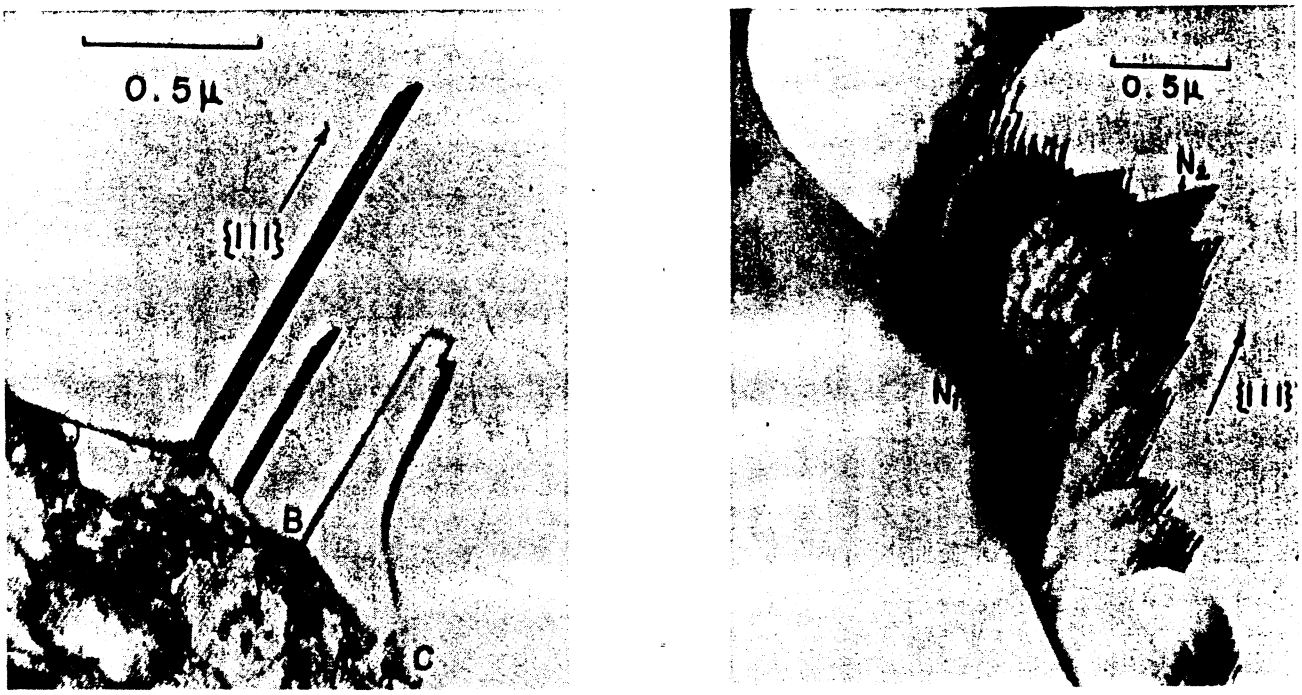

(a) (b)

Fig. 14 - (a) Grain boundary migrating into deformed material and leaving behind three annealing twins; (b) Packets of stacking faults at a grain boundary (From S. Dash and N. Brown, Acta Met., 11, 1067 (1963), Fig. 2(a) and 5(c), respectively).

Merklen et al. [48], in high voltage transmission electron microscopy experiments where in-situ recrystallization was produced, observed twins forming by Dash and Brown's mechanism. Figure 2 of Merklen et al. shows, clearly, features analogous to the ones presented in Figure 14(a). Hence, this is an established mechanism of annealing twin formation in recrystallization. They also observed an additional mechanism, which will be described in Section 4.

3.4 GRAIN-BOUNDARY DISSOCATION - This model was originally proposed as the "pop-out" model by Meyers and Murr [11], in 1978. Goodhew [49] observed specific instances of grain-boundary dissociation and proposed dissociation reactions. Grain-boundary dissociation takes place in order to decrease the overall interfacial energy. The mechanism of annealing twin formation by grain-boundary dissocation is shown in Figure 15. No associated grain-boundary migration is required and the boundary segment 12 decomposes into 13 and 32. If 13 is a coherent twin boundary and 12 is a non-coherent twin boundary we need:

$$\gamma_{gb} A_{12} > \gamma_{tb} A_{13} + \gamma_{ntb} A_{32} + \gamma_{sp} A_{12} \quad (9)$$

γ_{gb}, γ_{tb}, γ_{ntb}, and γ_{sp} are the energies of random, coherent twin, non-coherent twin, and special boundaries respectively. Dissociation is energetically favored if the new grain boundary 12 is a low-energy boundary. Meyers and Murr [11] suggested that this would be possible if the newly formed boundary were a "special" boundary. Goodhew, in a series of experiments on grain-boundary dissociation, found that they all occurred at coincidence site boundaries having values of $\Sigma 9$, $\Sigma 11$, and $\Sigma 99$ (Σ is the reciprocal density of coincidental sites throughout the coincidence site lattice). The following reactions were observed.

$$\Sigma 9 \rightarrow \Sigma 3 - \Sigma 3 \quad (10)$$

$$\Sigma 11 \rightarrow \Sigma 3 - \Sigma 33 \quad (11)$$

$$\Sigma 99 \rightarrow \Sigma 3 + \Sigma 33 \quad (12)$$

$\Sigma 3$ is a coherent annealing twin boundary. Notice that this mechanism does not require grain boundary migration per se. Once the grain boundary has dissociated, the non-coherent boundary, which was visualized as composed of the glissile interface of Figure 7(b), can migrate away from the grain boundary. This is shown in Figure 15(c). The processes of dissociation and migration were called initiation and propagation, respectively, by Meyers and Murr [11]. Growth can also proceed by migration of the grain boundary, obviously (Figure 15(d)). The propagation stage is shown in a clearer way in the three-dimensional representation of Fig-

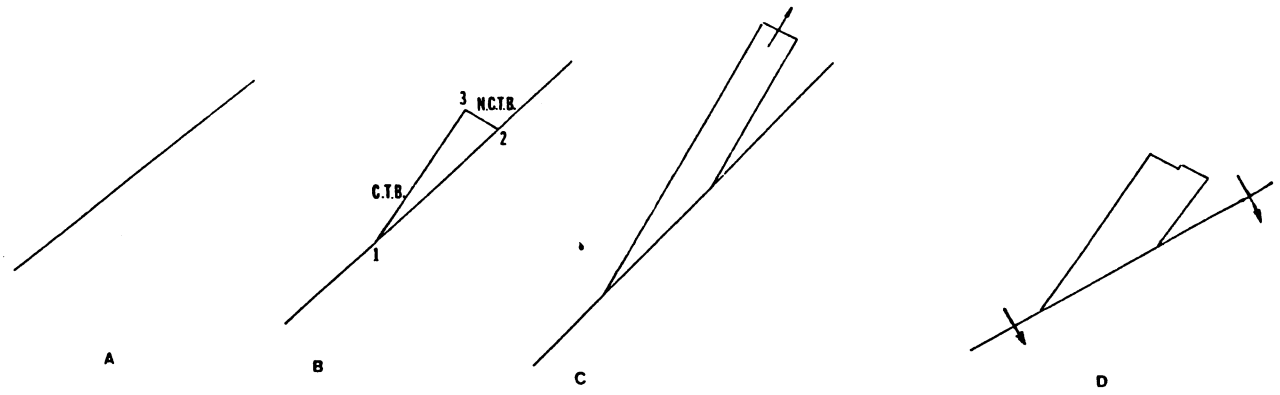

Fig. 15 - Annealing twin formation by grain boundary dissociation.

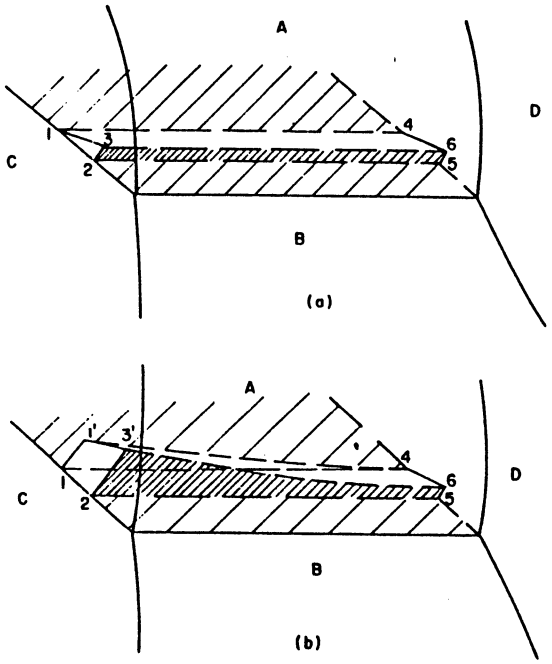

Fig. 16 - Three-dimensional representation of twin nucleus and incipient twin formation which appears as a ledge or double ledge in the grain boundary plane. (a) Small triangular nucleus . (b) Popping out of incipient twin along one portion of the grain boundary to form a partially grown annealing twin band (From M. A. Meyers and L. E. Murr, Acta Met., 26, 951 (1978), Fig. 3).

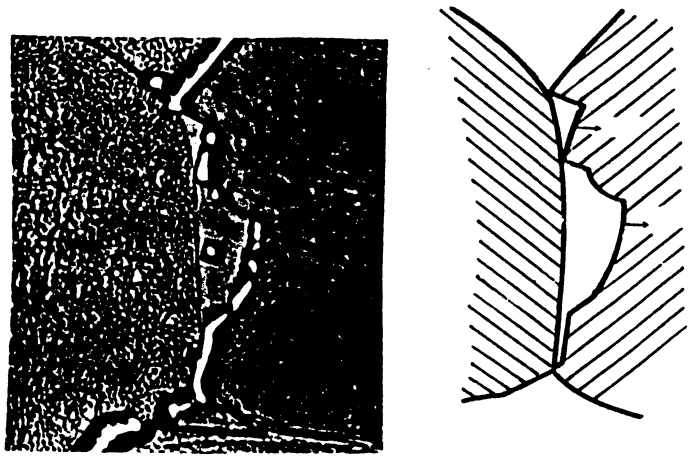

Fig. 17 - (a) Partially recrystallized nickel (recrystallized region is smooth with square pit in center) showing migration of grain boundary by movement of non-coherent twin boundary (From J. Hennaut, R. Pankowski, and M. G. Homes, Mem. Sci. Rev. Metall., 70, 151 (1973), Fig. 14); (b) Tracing of Fig. 19(a).

ure 16. The twin traverses the AB boundary entirely, and its limiting faces 123 and 456 are in direct contact with the adjoining grains C and D, respectively. 2365 and 1463 are the coherent and non-coherent twin boundaries, respectively, and the original boundary 1254 has vanished, or has been substituted by a 'special boundary'. The growth of the twin from its nucleus will proceed through the migration of the non-coherent twin boundary 1463, as shown in Figure 16(b). Again, the driving energy for the process will be the reduction of the overall interfacial energy and dislocation density (if recovery has not been completed). The energy of the non-coherent twin boundary depends on its inclination. By rotating it conveniently, it will fall into one of the 'special boundary' orientations. Indeed, the non-coherent twin boundaries have been found to have preferential orientations. The energy gradient provides a torque that tends to rotate the non-coherent twin boundary away from its nucleus inclination. Figure 16(b) shows the growth of the twin under the influence of the combined driving energies. The growth takes place by migration of the non-coherent twin boundary; this assures a relatively low energy expenditure in the formation of the lateral boundaries 23'65 and 11'4, since

they are coherent twin boundaries. However, the separation between the parallel coherent boundaries is not expected to change during the propagation stage; it is thought that the mobility of coherent twin boundaries in a direction perpendicular to the boundary is much lower than that of random boundaries. If the growth is taking place during recovery, the sweep-up of dislocations inside the twinned volume provides a source ofdriving energy. The growth will be completed when a minimum level of energy is reached.

Since the non-coherent twin boundary represents the interface between two lattices with high coincidence (one in three) it is a low energy boundary even when it is not exactly at a 'special orientation'. Measurements of the non-coherent grain boundary energy systematically show lower energies than random grain boundaries. Aust and Rutter [50-52] showed, for pure lead, that while the migration rates of random and special boundaries were identical, the addition of small amounts of tin affected the migration rates of random boundaries much more than special boundaries. The results indicate that the solute atoms segregate more in the random than in the special boundaries, hindering the mobility of the former ones. Evidence for this preferential segregation at random boundaries is presented by Gleiter [53]. It can be concluded from the above that the non-coherent boundary, once it 'pops out' of the grain boundary, has a higher mobility than the surrounding grain boundaries. Its migration--and the associated twin propagation--could therefore proceed at temperatures below the recrystallization temperature. Evidence for grain-boundary dissociation has also been given by early experiments conducted by Hennaut et al. [54]. They used a special etching technique that revealed (through pits) the crystallographic orientation of surfaces in nickel. They could also differentiate between deformed and recrystalized regions. The optical micrograph of Figure 17 shows the formation of an annealing twin in a partially recrystallized specimen. The recrystallized region is smoother and has a square pit in its center. Figure 17(b) is a tracing, showing how the recrystallization front is moving. Deformed material is indicated by hatching. It is clear that recrystallization is proceeding by the advance of the non-coherent boundary, in accord with the grain-boundary dissociation mechanism. The recrystalized region is distinguished from the deformed matrix by its smoother surface. However, Hennaut et al. [54] also observed different mechanism, discussed in Section 4.

4. ADDITIONAL OBSERVATIONS AND ANALYSES

It is important to separate annealing twins into recrystallization, grain growth, and solidification twins. A number of recent transmission electron microscopy studies, especially using high voltages, have revealed the details of recrystallization through in-situ observations. These studies are demonstrating the importance of "recrystallization" twinning in texture formation. These observations and possible interpretations are discussed in Section 4.1. Quantitative information on annealing twin occurence, on the other hand, is scant in the literature. Some of the significant results are reviewed in Section 4.2.

4.1 OBSERVATION OF "RECRYSTALLIZATION" TWINS - Observations by several investigators will be reviewed in this section. Burke [37], in 1950, made the first observation of a recrystallization twin. A tracing from his Figure 2 is shown in Figure 18. The hatched region indicates deformed alpha brass. At a magnification of 2000X, Burke was able to identify a small recrystallized region containing the three twins. Transmission electron microscopy evidencing the sequence leading to the formation of recrystallization twins is shown in Figure 19, from Merklen et al. [48]. Merklen et al. [48]

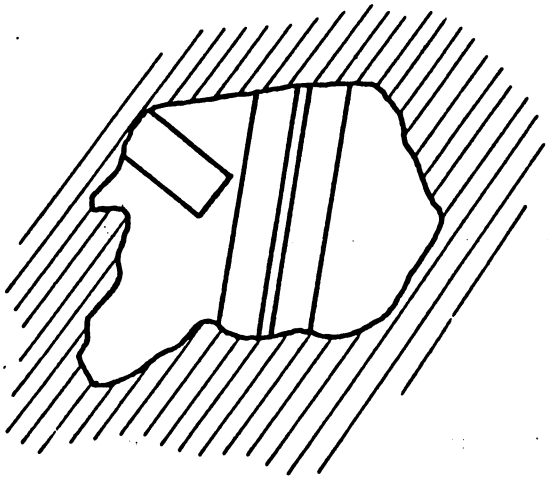

Fig. 18 - Recrystallized grain growing into deformed matrix in copper (2000 X) (From J. E. Burke, Trans. AIME, 188, 1324 (1950), Fig. 2).

obtained this sequence by in-situ recrystallization in a high-voltage transmission electron microscope. It shows a recrystallized grain in nickel in the process of growth. In Figure 19(a), A and B are at twin orientation. In Figure 19(c), region labeled C has formed; it is in twin orientation with A. The twin boundaries formed in this manner are approximately parallel to the recrystallization boundaries. Earlier, Votava and Hatwell [55] observed similar annealing twin patterns in copper that was partially recrystallized. Peters [56], in 1972, studied recrystallization in heavily deformed bronze and found that annealing twins played a prominent role in texture formation during recrystallization. He observed that ". . . the change in texture may be associated with the formation of twins which happen to be oriented such that they can grow more rapidly than the original nuclei." He proposed the scheme shown in Figure 20 for the formation of the recrystallized material. First, small recrystallized nuclei are formed by polygonization (Figure 20(b)). Twins (T) form along these nuclei and grow (Figure 20(c)). These twins, in turn, form other twins, called second generation twins. They are marked 2 in Figure 20(d). Primary recrystallization is complete in Figure 20(f).

Ralph, in a review article on grain boundaries [57], shows a boundary in the process of recrystallization, with a number of twins being produced. This is shown in Figure 21. The deformed region is at the bottom of the micrograph and the recrystallized region at the top. The dark field micrograph illuminates the twins of a single variant, as shown in Figure 21(b). These twins clearly have formed by Dash and Brown's mechanism.

Slakhorst [58] performed recrystallization experiments in high purity silver and a series of Ni-Co alloys and found that recrystallization twins played a major role in texture formation.

Rae et al. [59] recently investigated texture formation and calculated orientations after first, second, and up to 12th generation twins in recrystallization. They also performed observations by transmission electron microscopy showing multiple recrystallization twin formation as the recrystallization front propagated throughout the material. These observations were made in a 1 MeV transmission electron microscope in cold rolled copper thin foils. Rae et al. [59] state that "Multiple twinning has been known to occur and hence produce a relatively mobile boundary, from an interface that was initially migrating very slowly". Taylor et al. [61] determined the recrystallization texture of copper-silica. In-situ annealing observations in the high voltage electron microscope revealed that the most prominent feature of the recrystallized grain structure was the large number of twins. Their Figure 10 illustrates the modified growth accident proposed later in this section.

Additional instances of twin formation during recrystallization can be found in the work

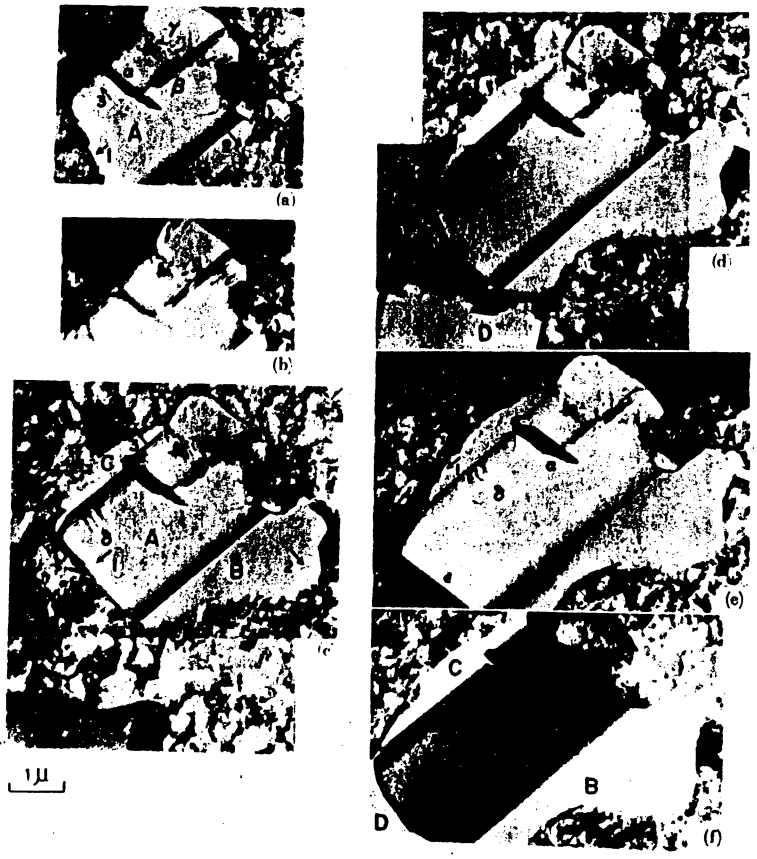

Fig. 19 - Successive stages of parallel-sided twin formation in the course of primary recrystallization (From P. Merklen, E. Furubayashi, and H. Yoshida, Trans. J.I.M., 11, 252 (1970), Fig. 1).

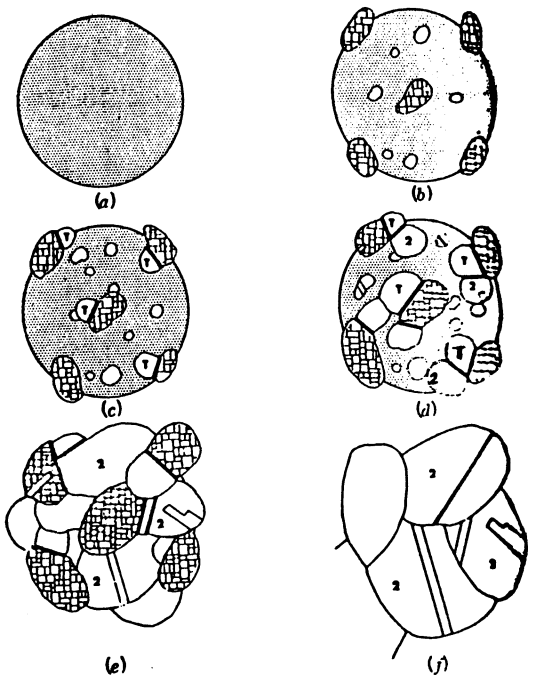

Fig. 20 - Schematic drawing showing the formation of nuclei by polygonization (B), the growth of twins "T" and second generation twins "2", primary recrystallization (E), and grain growth with second-generation twins dominating (From B.F. Peters, Met. Trans., 4, 757 (1973)).

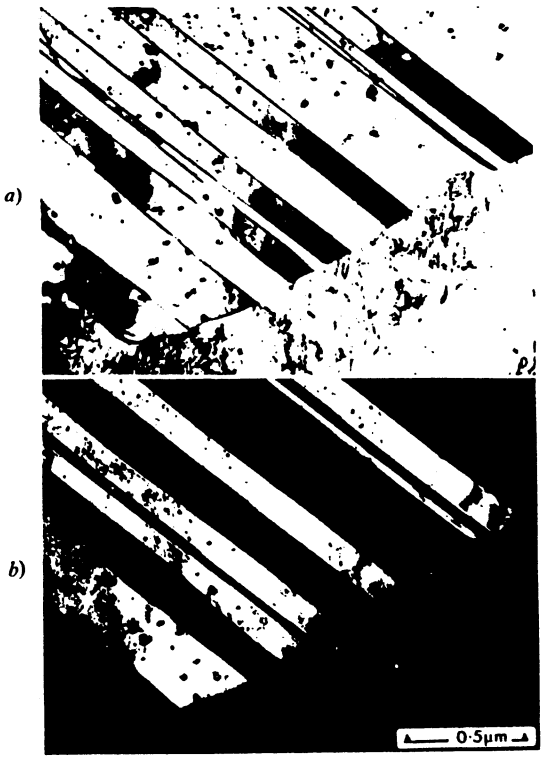

Fig. 21 - Bright-field (a)/dark-field (b) pair of single variant back twinning from a recrystallizing interface in 20/25 stainless steel (From B. Ralph, J. de physique, (Colloque C4), 36, C4-71 (1975)).

of Jones [60] and Wilbrandt and Haasen [62]. These observations are shown in Figures 22 through 24. In Figure 22 the twin T_1 is growing into the deformed metal by the migration of the non-coherent twin boundary. The arrow indicates the growth direction. In Figure 23 a small twin pocket separates the recrystallized grain 1 from deformed grain 2. The twin is shown clearly in the dark field micrograph of Figure 23(b).

Figure 24 shows tracings adapted from Wildbrandt and Haasen [62]. These investigators performed in-situ recrystallization experiments on copper monocrystals deformed to a strain of 80 percent. The formation of annealing twins determines the orientation of the recrystallization texture, according to Wildbrandt and Haasen [62]. The two structures depicted in Figure 24 represent the formation of recrystallization twins having their coherent twin boundaries approximately perpendicular (a) and parallel (b) to the migrating recrystallization front. The deformed material is hatched in the tracings, and the recrystallization front is moving into the deformed material. The most plausible explanation for the formation of the recrystallization twins in Figure 24(a) is by Dash and Brown's mechanism, while the twins of Figure 24(b) seem to be formed by a fault mechanism, described in greater detail below.

The observations presented in this section indicate that recrystallization twins can form by a pop-out mechanism, by Dash and Brown's mechanism, or by a third, more common mechanism. This seems to be a growth fault mechanism. It is, however, different from the one proposed by Fullman and Fisher [40], and a possible sequence will be proposed here (Figure 25). The critical element of this modified growth accident model is that nucleation starts at the region in boundary where a (111) plane would be tangent to the boundary surface. This allows the initial length of the coherent twin boundary to be zero; it is shown in Figure 25(b). The formation of the coherent twin creates a boundary of enhanced mobility (and lower energy). As this boundary advances ((c) and (d)), the length of the coherent twin boundary increases. A second fault will create a parallel-sided twin (Figure 25(e)). The migrating boundary will apply a

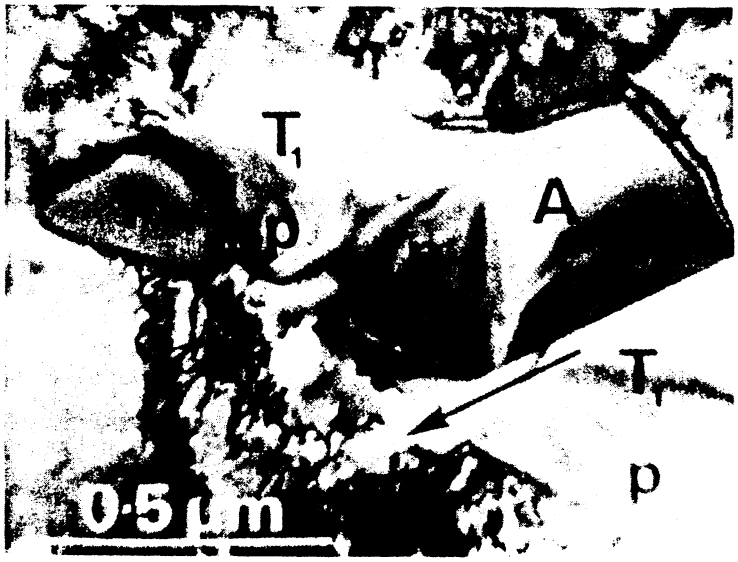

Fig. 22 - Recrystallization nucleus forming in AFS ± 310 stainless steel; parallel-sided twin A separates two regions T_1. T_1 on lower right-hand side growing into deformed grain by migration of non-coherent grain boundary (From A. R. Jones, J. Matls. Sci., 16, 1374 (1981), Fig. 3).

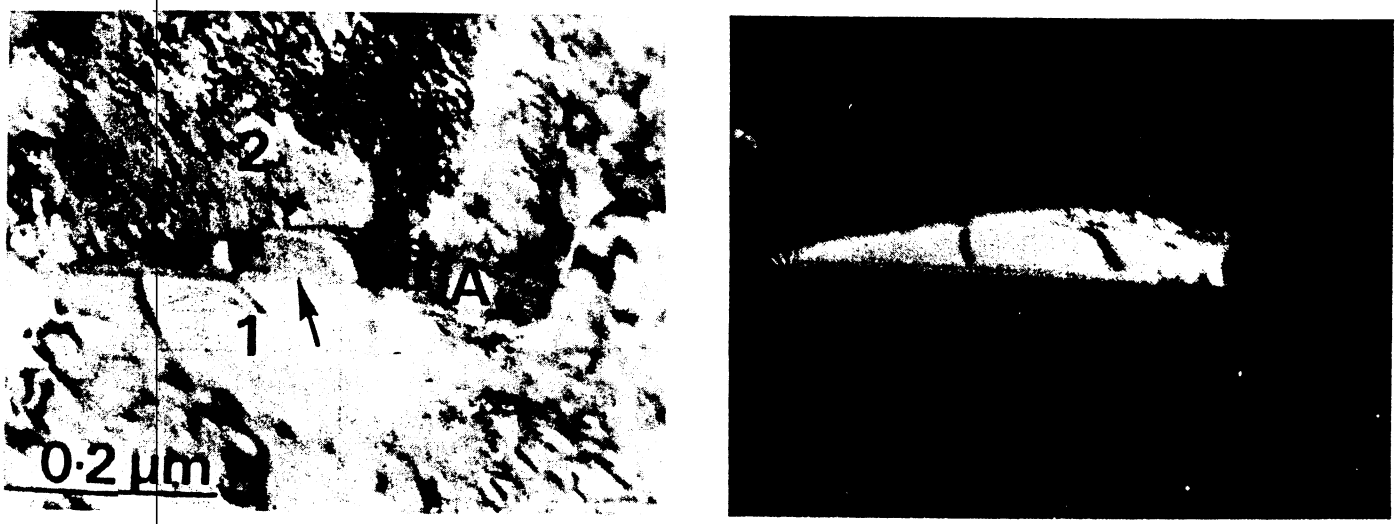

(a) (b)

Fig. 23 - Coherent twin boundary in recrystallized grain in AISI 310 stainless steel. (a) bright-field; (b) dark field through diffraction spot of upper region (From A. R. Jones, J. Matls. Sci., 16, 1380 (1981), Fig. 1).

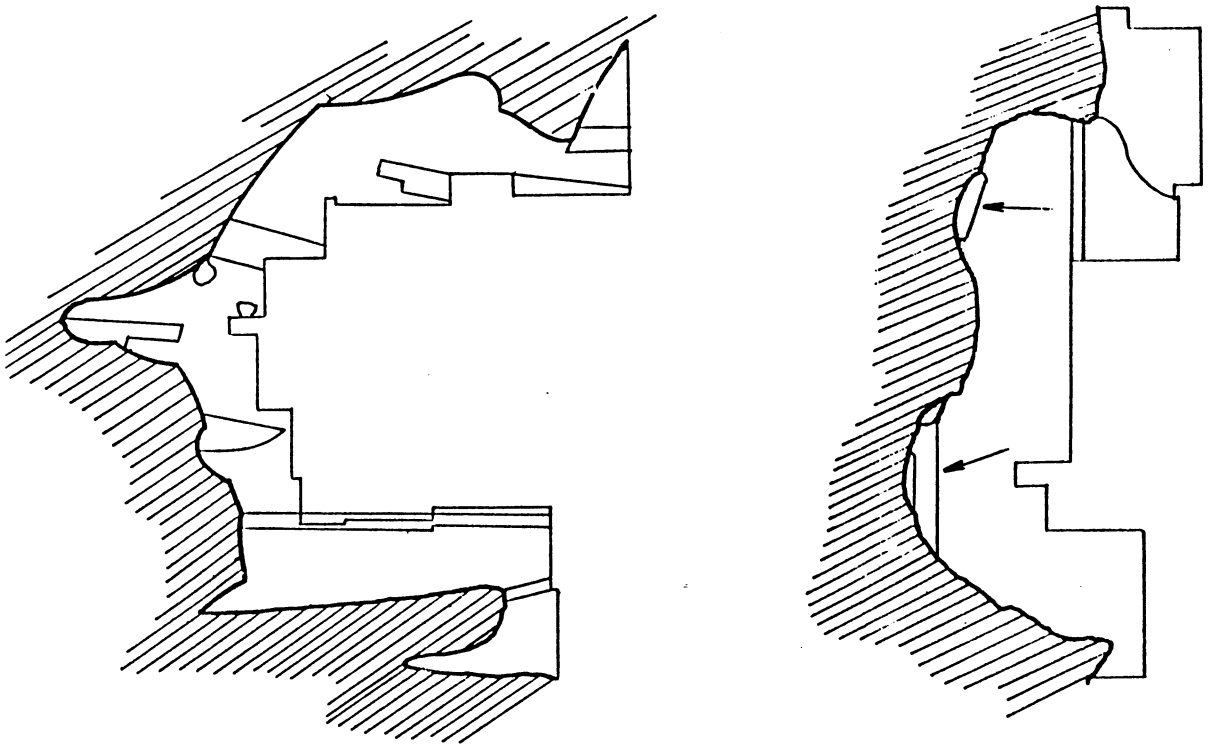

Fig. 24 - Tracings of advancing recrystallization front (deformed material hatched) in high purity copper observed in high-voltage transmission electron microscope. (a) coherent twin boundaries at angle close to 90° to advancing recrystallization front, (b) coherent twin boundaries nearly parallel to advancing recrystallization front. (Adapted from P.-J. Wilbrandt and P. Haasen, Z. Metallkde., 71, 385 (1980), Fig. 2(b) and 3(b), respectively).

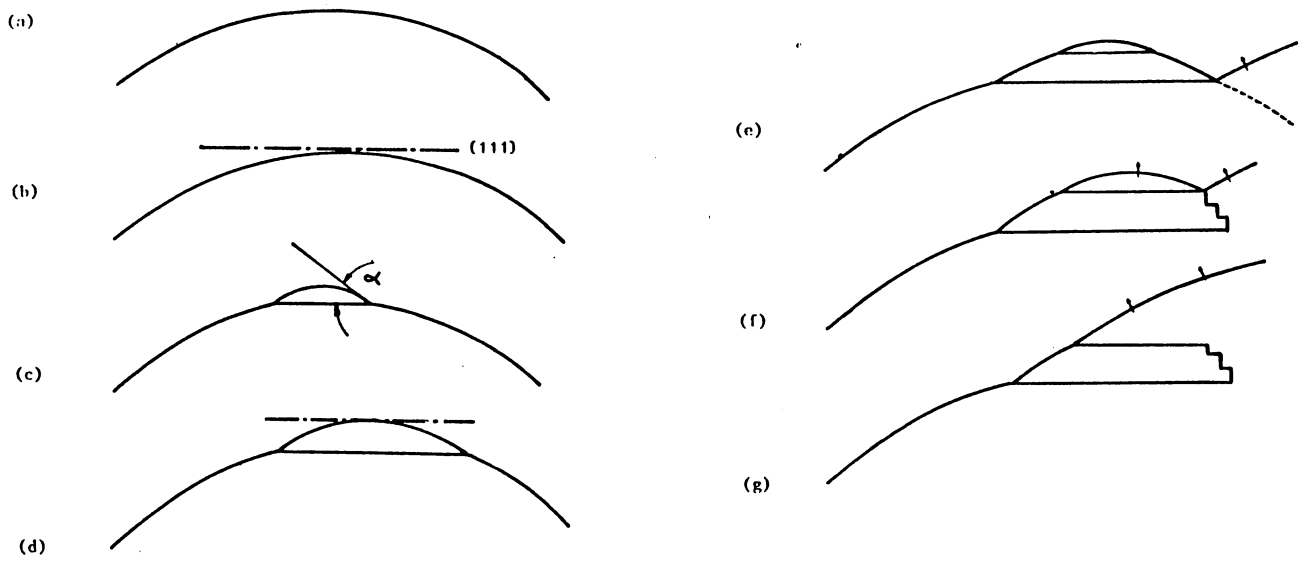

Fig. 25 - Modified growth accident model in which twin boundary nucleates at tangency point between migrating boundary and (111).

tension on the coherent twin boundary, which may lead to the dissociation of the grain boundary (Figure 25(f)), leading to the freeing of the boundary from the twin. This allows the continuation of the recrystallization process, with the formation of a non-coherent twin boundary. It also explains why twins are most often found in pairs. The boundary shown in Figure 25(g) will not nucleate an additional twin boundary parallel to the other two because it does not meet the tangency requirement. This tangency requirement is thought to be critical for the understanding of parallel-sided twins. Non-parallel twins will only be formed if α (Figure 25(c)) exceeds 74.54^{o} when the new twin is nucleating. This will be discussed in greater detail in a forthcoming paper.

4.2 QUANTITATIVE MEASUREMENTS OF TWINS - The interpretation of quantitative measurements on annealing twins has been marred by confusion. One of the reasons is that twin density measurements have been made using different techniques. At least four different measurement schemes have been used:

(a) Twins per grain: the number of annealing twin boundaries per grain is measured, on a cross-section. This is, obviously, not a rigorous measure of the true number of annealing twin boundaries per grain, but is directly related to it.

(b) Twins per area. The number of twins per unit area of section is counted. This measure lacks rigor, since a twin boundary represents a surface and what is being measured is the number of surfaces intersecting an area.

(c) Twins intersecting a unit length line. This is the linear intercept method, which can lead to a direct measure of the total twin area per unit volume.

(d) Areal fraction of twins (= vol. fraction). This assumes that the twinned volume is the region between two parallel coherent twin boundaries.

Form et al. [63] discuss the relative merits of these measurement techniques.

Pande et al. [41] measured twin width as a function of grain size and found the proportional relationship shown in Figure 26. The twin width was found to be equal to approximately one third of the average grain size D. It is not known whether this ratio is dependent upon the amount of previous cold work. This constancy demonstrates that annealing twins are eliminated and re-created, as grain growth proceeds. Materials annealed at higher temperatures will exhibit wider annealing twins. Results by Form et al. [63] indicate that for Cu and Cu-Al alloys the annealing twin density increases with cold work, while for nickel this factor is approximately constant.

The quantitative measurements conducted by Vohringer [64] are of considerable significance. He determined the annealing twin concentration (twins per grain) as a function of grain size for a number of alloys. He was able to do this at a constant grain size of 50μm and the results are shown in Figure 27. The consistency between different alloys is excellent with the exception of silver. He points out that the results for silver are taken from the literature and this could be the reason for the inconsistency. In Figure 27 the abscissa represents a normalized parameter γ/Gb, where γ is the stacking-fault

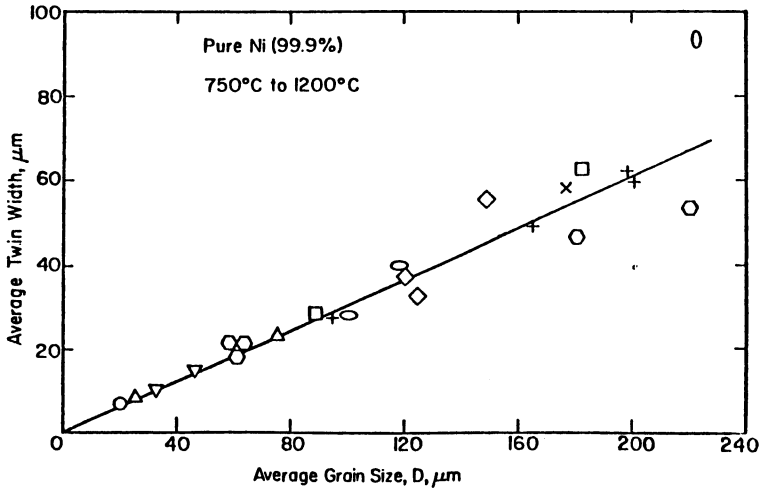

Fig. 26 - Relationship between twin width and grain size for nickel (99.9%) (From C.S. Pande, M. A. Imam, and B. B. Rath, unpublished results).

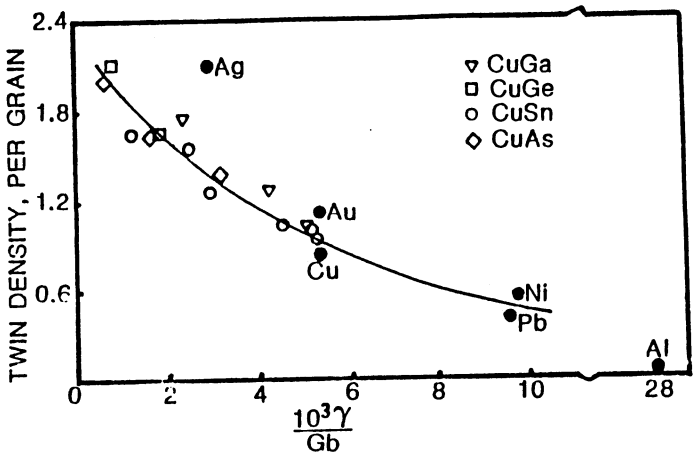

Fig. 27 - Relationship between annealing twin density (counted as number of annealing twin boundaries per grain) and stacking fault energy, at constant grain size of 50 μm for FCC metals and alloys (From O. Vöhringer, Metall, 11, 1119 (1972), Fig. 9).

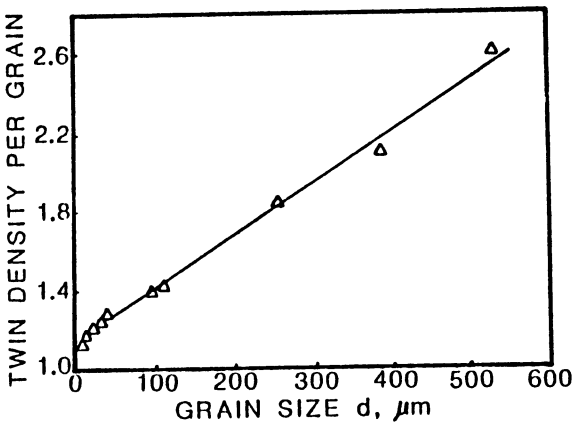

Fig. 28 - Annealing twin density (in twins/grain) as a function of grain size for Cu-15 at% Zn alloy (From O. Vöhringer, Metall, 11, 1119 (1972), Fig. 7).

energy, G is the shear modulus, and b is the Burgers vector. By expressing analytically Vohringer's [64] plot, we arrive at:

$$Z_r = 2.25 \exp(-165\,\gamma/Gb) \qquad (13)$$

By using an appropriate expression for the grain-size dependence of annealing twin density it is possible to develop a generalized equation. A preliminary attempt is made below. Vohringer [64] also measured the change in an nealing twin density (Z_r) with grain size. For Cu-15 at % Zn, he found a linear increase of Z_r with grain size. Figure 28 shows the results. The annealing twin density increases from 1.2/grain for 30 μm grain size to 2.6/grain for 540 μm grain size. This is a significant increase. However, other alloys did not exhibit such an increase. Compte and Form [65] report an increase in the number of twins per grain with increasing recrystallized grain size. Adeev and Petrov [66] determined the annealing twin density in Fe-C alloys in the austentic range (950 - 1050°C) and found that it increased with increasing grain size. Experiments conducted by these authors for Ni-200 cold rolled to 90 percent reduction and annealed at different temperatures confirm the grain-size dependence of annealing twin density. These differences are illustrated in Figure 29. The microstructures after two annealing treatments (800°C/1 hour and 1100°C/1 hour) are shown. The two micrographs were taken at different magnifications to show the grains at approximately the same size; the difference in annealing twin

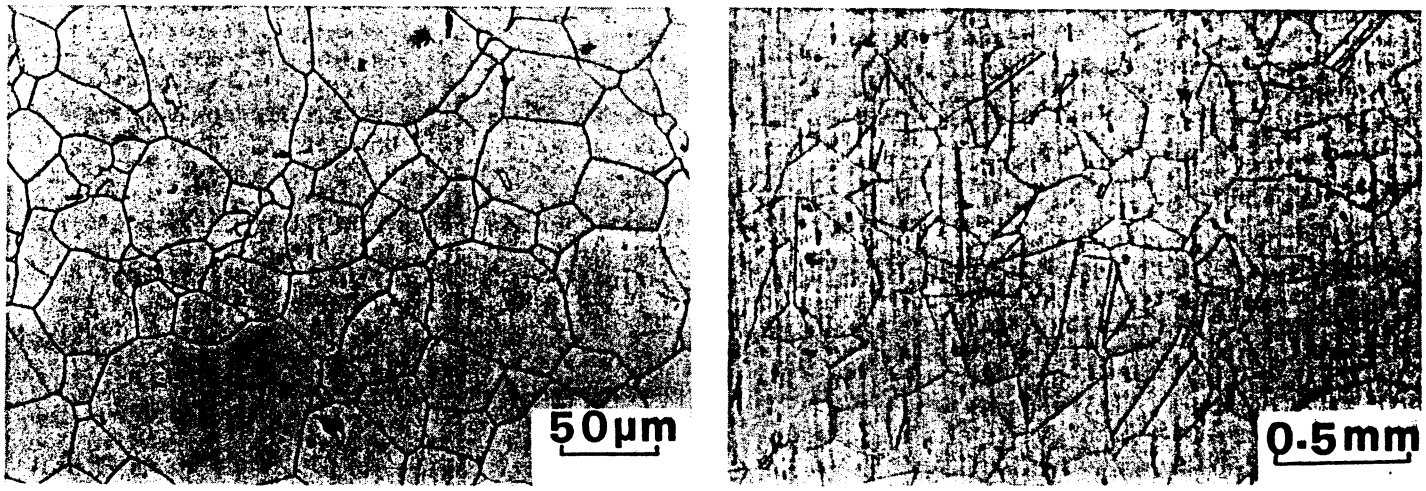

(a) (b)

Fig. 29 - Microstructures of Ni-200 cold-rolled 90 pct and then annealed for one hour at (a) 800°C and (b) 1100°C.

density is clearly evident. The incidence of annealing twins is much more prevalent in Figure 29(b). Quantitative measurements were made and the results are shown in Table IV.

TABLE IV

Density of Twin Boundaries (Z_r) for Ni-200 Cold Rolled to a 90 pct. Reduction and Annealed

Annealing Temperature	Annealing Time			
	10 min.		1 hour	
(°C)	Grain Size (µm)	Z_r	Grain Size (µm)	Z_r
700	7.6		7.7	0.41
800	14	0.27	26	0.16
900	38	0.33	66	1.06
1000	78	0.51	120	0.96
1100	120	0.55	120	1.72

Care was taken to make observations only after a substantial layer was removed. Surface effects, such as pinning of boundaries, could interfere. In spite of the wide scatter in the data, it is evident that the density increases with time, at a certain temperature, for Ni-200. This is consistent with Figure 29. Measurements made after 30 min. anneals yielded similar results.

One can consider the annealing twins as being the result of the recrystallization and grain-growth processes:

$$Z_r = Z_{rec} + Z_{gg} \qquad (14)$$

In grain growth, one can confidently say that the Dash and Brown grain-boundary dissociation and growth accident models operate, and that twins form as grain boundaries migrate. Hence, the twin density is proportional to the average distance migrated by a grain boundary during grain growth. Assuming that recrystallization produces a density of Z_{rec} and a recrystallized grain diameter D_o, and that the final grain size is D, one has:

$$Z_r = Z_{rec} + C \left(\frac{D - Do}{2} \right) \qquad (15)$$

C is a constant (related to the twin fault probability) and $(D-D_o)/2$ is the mean distance traveled by a grain boundary during grain growth. In Figure 28, one would have, applying the equation above:

$$Z_r = 1.1 + 2.8 \times 10^{-3} \left(\frac{D-10}{2} \right) \qquad (16)$$

This relationship does not incorporate an annihilation factor. It assumes that a specific grain grows from recrystallization without being traversed by any other grain boundary. Hence, the recrystallization twins are conserved in it. The model could be improved by introducing this effect. Assuming that existing annealing twins are annihilated when a grain boundary passes through them, an annihilation rate could be established from the average number of grain boundaries that pass through an arbitrary point during grain growth.

From the discussion above, it is clear that there is, at present, no theory which accounts for the experimental observations. It seems that, from a mechanistic point of view, the best measure of annealing twins is their number per grain. The change in density with grain size is due to the net balance between generation and

annihilation of annealing twins, assuming that coherent annealing twin boundaries are immobile. The combined use of Equations 13 and 15 provides twin-boundary densities for different materials. However, Z_{rec}, C and D_o have to be experimentally determined, and therefore this is not truly a predictive theory.

4.3 THE ICOSAHEDRAL PHASE - The recent discovery of an icosahedral phase by Shechtman et al. [67] has attracted considerable attention in the materials community. Annealing (solidification) twins might play an important role in the formation of the "pentagonal" symmetry, as will be shown here. Hillert and Agren [68] proposed a growth mechanism for the icosahedral phase based on twinning. Actually, Pangarov [69], in 1977, discusses in detail the formation of silver crystals containing this five-fold symmetry. By applying a pulse potentiostatic technique and depositing silver crystals on a platinum substrate from a cyanide solution, Pangarov [69] obtained five-fold symmetry crystals when the overvoltage was high. As the overvoltage increased, so did the twin density. His explanation is simple. The angle between (111) planes and twin planes is 70.54°. By multiplying this by five, one obtains 352.7°. This is 7.3° less than the full 360° rotation.

The same argument is developed by Hillert and Agren [68]. Figure 30 shows the pentagonal scheme proposed by Pangarov [69] and the corresponding array of (111). Thus, the icosahedral structure is originated at the confluence of five annealing twin boundaries, intersecting along one common axis ([110]). One of the boundaries has a misfit of 7.3°. This can be easily accomodated by a tilt boundary dislocation array. The spacing between the dislocations along this tilt boundary will be:

$$d \simeq \frac{b}{2 \sin \left(\frac{\theta}{2}\right)} = 7.85b \simeq 8b \qquad (17)$$

One such dislocation is shown in Figure 30(b). It corresponds to the eigth plane (counting from the origin). It is also possible that the distortion is evenly distributed among the five planes. In this case, the angular distortion is equal to 1.46° per twin plane. This corresponds to approximately one dislocation for every 39 planes.

The icosahedral phase found by Schectman et al. [67] seems to be truly a "quasicrystal", since it has the characteristic electron diffraction pattern, even when a convergent beam is used (20 nm diameter). Thus, the structure

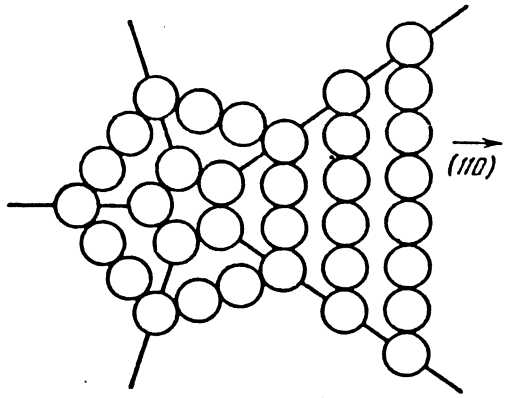

(a)

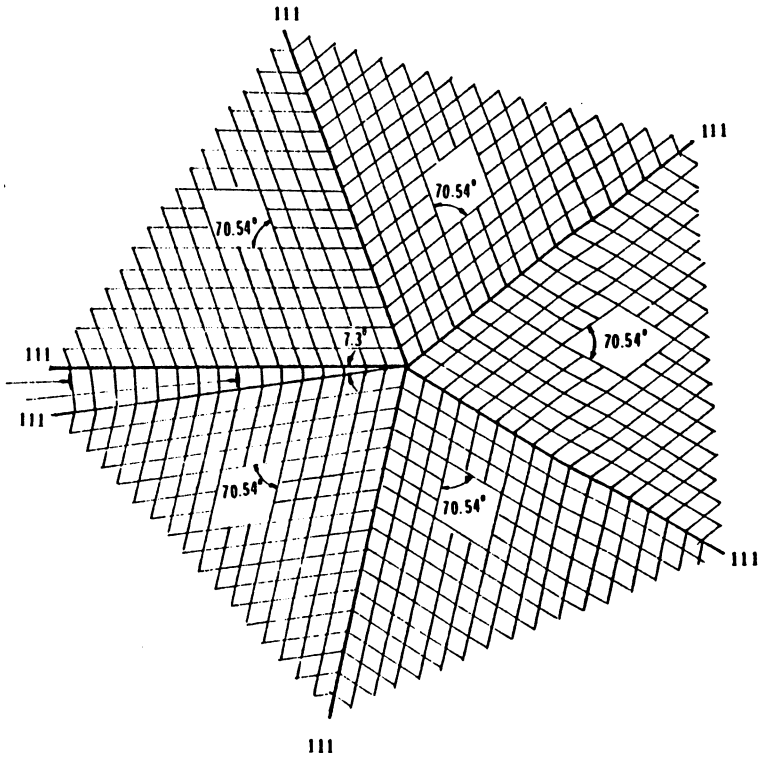

(b)

Fig. 30 (a) Growth of crystal with five-fold symmetry according to Pangarov [69]; (b) representation of (111) planes in five confluent twin-oriented grains and tilt boundary superimposed on coherent twin boundary.

presented in Figure 30 is not not necessarily that of the icosahedral phase. The size of the units shown in Figure 30 would have to be very small in order for the electron diffraction pattern to show the icosahedral symmetry.

5. CONCLUDING REMARKS

a) Annealing twins should be divided into recrystallization, grain-growth, and solidification twins.
b) Recrystallization twins are very important in that they determine the structure of the recrystallized material (low and medium stacking fault energy FCC metals).
c) One single mechanism cannot explain the formation of all twins. There is documented evidence for Dash and Brown's mechanism, grain-boundary dissociation mechanism, and a growth-fault mechanism (both the Fullman Fisher version or modifications proposed by Gleiter and in Figure 25).
d) In recrystallization, twins form to generate interfaces that have greater mobility. Successive generations of twins can thus form, as the recrystallization front moves into deformed (and distorted) material.
e) There is a definite need for quantitative treatments of annealing twin densities that predict the observed density changes with grain size, composition, etc.
f) The best measure of annealing twin densities is the determination of twins per grain.
g) The modified growth accident model presented in this manuscript (Figure 25) explains the occurrence of parallel-sided twins, which are the great majority for low and medium stacking-fault energy metals and alloys.

ACKNOWLEDGEMENTS

This research was funded by National Science Foundation Grant No. DMR 8115127 and by the Center for Explosives Technology Research. The help of Mr. S. N. Chang in the preparation of the manuscript is greatly appreciated.

REFERENCES

1. H. Carpenter and S. Tamura, Proc. R. Soc. (A), 113, 161 (1926).
2. G. Gindraux and W. Form, J. Inst. Metals, 101, 85 (1973).
3. S. R. Rouze, Microstructures, 2, No. 6, 26 (1971).
4. R. L. Fullman, J. Appl. Phys., 22, 456 (1951).
5. C. M. Sargent, Trans. Metall. Soc. AIME, 242, 1183 (1968).
6. P. R. Howell and J. V. Bee, J. Mat. Sci., 13, 1583 (1978).
7. D. Vaughan, Phil. Mag., 22, 1003 (1970).
8. L. E. Murr, R. J. Horylev, and W. N. Lin, Phil. Mag., 20, 1245 (1969).
9. L. E. Murr, R. J. Horylev, and W. N. Lin, Phil. Mag., 22, 515 (1970).
10. J. M. Oblak and B. H. Kear, Proc. 28th Annual Meeting of EMSA, 1970, p. 432.
11. M. A. Meyers and L. E. Murr, Acta Met., 26, 951 (1978).
12. M. J. Carr, Sandia National Laboratories, private communication (1985).
13. V. M. Kosevich, V. Ya. Lunkin, and A. A. Udovenko, Phys. of Met. and Metallogr., 46, 146 (1978).
14. H. Gleiter, Acta Met., 17, 565 (1969).
15. L. E. Murr, Acta Met., 21, 791 (1973).
16. V. O. Yesin, I. G. Brodova, G. N. Pankin, and I. P. Korshunov, Phys. Met. Metallogr., 50, 190 (1980).
17. J. Gastaldi and C. Jourdan, Phys. Stat. Sol., 52, 139 (1979).
18. J. T. McGinn, V. A. Greenhut, and T. Tsakalakos, Acta Met., 30, 2103 (1982).
19. A. S. Bay, Y. S. Sollertinskaya, L. I. Tvorogova, and S. S. Khayutin, Phys. of Met. and Metallogr. 33, 213 (1972).
20. C. T. Liu, Intl. Metals Reviews, 29, 168 (1984).

21. P. Tardy and S. S. Iskander, J. Matls. Sci. 4, 353 (1969).

22. J. A. Eady and W. C. Winegard, Met. Trans., 5, 2246 (1974).

23. C. J. Simpson, K. T. Aust, and W. C. Winegard, Met. Trans., 1, 1782 (1970).

24. E. M. Schulson, T. P. Weihs, D. V. Viens, and I. Baker, Acta Met., 33, 1587 (1985).

25. K. Z. Saleeb and S. Kadeckova, Krist. and Tech. (Germany), 9, 1265 (1974).

26. R. W. Cahn and J. A. Coll, Acta Met., 9, 138 (1961).

27. E. M. Schulson, Intl. Metals Reviews, 29, 195 (1984).

28. M. Viltange, C. R. Hebd. Seances Acad. Sci. (France), 280, No. 3, 69 (1975).

29. D. S. Hutton, G. L. Coleman, and W. C. Leslie, Trans. Met. Soc. AIME, 215, 680 (1959).

30. A. Fourdeux and A. Berghezan, J. Inst. Met., 89, 31 (1960).

31. E. B. Simonsen, Acta Met., 10, 172 (1962).

32. R. J. Wasilewski, Acta Met., 14, 433 (1966).

33. R. L. Segall, Acta Met., 9, 975 (1961).

34. W. N. Borle, Scripta Met., 7, 267 (1973).

35. I. Ohdomari and N. Onoda, Phil. Mag., 35, 1373 (1977).

36. A. G. Guy and J. J. Hren, Physical Metallurgy, Addison Wesley, Reading, Mass., p. 302.

37. E. Burke, Trans. Am. Inst. Min. Eng., 188, 1324 (1950).

38. H. Gleiter, Acta Met., 17, 1421 (1969).

39. G. Baro and H. Gleiter, Zeitsch. fur Metallkde. 63, 661 (1972).

40. R. L. Fullman and J. C. Fisher, J. Appl. Phys., 22, 1350 (1951).

41. C. S. Pande, M. A. Iman, and B. B. Rath, Naval Research Laboratory, unpublished research.

42. J. T. McGinn, V. A. Greenhut, T. Tsakalakos and J. Blane, Acta Met., 30, 2093 (1982).

43. J. P. Nielsen, Acta Met, 15, 1083 (1967).

44. W. G. Burgers, Nature, London, 157, 76 (1946).

45. W. G. Burgers, Physica, 15, 92 (1949).

46. S. G. Khayutin, Phys. Metal. Metalloved., 29, 1316 (1970).

47. S. Dash and N. Brown, Acta Met., 11, 1067 (1963).

48. P. Merklen, E. Furubayashi, and H. Yoshida, Trans. Japan Inst. of Metals, 11, 252 (1970).

49. P. J. Goodhew, Metal Science, March, 108 (1979).

50. K. T. Aust and J. W. Rutter, Trans. Met. Soc. AIME, 215, 820 (1959).

51. K. T. Aust and J. W. Rutter, Trans. Met. Soc. AIME, 215, 119 (1959).

52. K. T. Aust and J. W. Rutter, Trans. Met. Soc. AIME, 218, 682 (1960).

53. H. Gleiter, Acta Met. 18, 117 (1970).

54. J. Hennaut, R. Pankowski, and M. G. Homes, Mem. Sci. Rev. Met., 70, 151 (1973).

55. E. Votava and H. Hatwell, Acta Met., 8, 874 (1960).

56. B. F. Peters, Met. Trans., 4, 757 (1972).

57. B. Ralph, J. de Physique, (Collogue C4); 36, C4-71 (1975).

58. J. W. H. G. Slakhorst, Acta Met., 23, 301 (1975).

59. C. M. F. Rae, C. R. M. Grovenor, and K. M. Knowles, Z. Metallkde., 72, (1981).

60. A. R. Jones, J. Matls. Sci., 16, 1374 (1981).

61. J. D. Taylor, R. E. Smallman, and B. J. Duggan, Metal Sci., 16, 411 (1982).

62. P. J. Wilbrandt and P. Haasen, Z. Metallkde. 71, 385 (1980).

63. W. Form, G. Gindraux, and V. Mlyncar, Metal Sci., Jan., 16, (1980).

64. O. Vohringer, Metall, 26, 119 (1972).

65. P. A. Compte and W. Form, Mem. Sci. Rev. Metall., 74, 339 (1977).

66. V. M. Adeev and Yu. N. Petrov, 20, 2004 (1975).

67. D. Shechtman, I. Blech, D. Gratias, and J. W. Cahn, Phys. Rev. Letters, 53, 1951 (1984).

68. M. Hillert and J. Agren, Acta Met., 33, 1621 (1985).

69. N. A. Pangarov, in "Growth of Crystals", Vol. 10, ed. N. N. Sheftal, Consultants Bureau, (a division of Plenum) New York and London, 1976, p. 62.